การดัดแปรพลาสมาโฟกัสสำหรับการปรับสภาพผิววัสดุ

นายดุสิต งามรุ่งโรจน์

วิทยานิพนธ์นี้เป็นส่วนหนึ่งของการศึกษาตามหลักสูตรปริญญาวิทยาศาสตรมหาบัณฑิต
สาขาวิชาฟิสิกส์ ภาควิชาฟิสิกส์
คณะวิทยาศาสตร์ จุฬาลงกรณ์มหาวิทยาลัย
ปีการศึกษา 2545
ISBN 974-17-1449-1

PLASMA FOCUS MODIFICATION FOR MATERIAL SURFACE TREATMENT

DUSIT NGAMRUNGROJ

A Thesis Submitted in Partial Fulfillment of the Requirements
for the Degree of Master of Science in Physics
Department of Physics
Faculty of Science
Chulalongkorn University
Academic Year 2002

ISBN 974-17-1449-1

Thesis Title	Plasma Focus Modification for Material Surface Treatment
By	Dusit Ngamrungroj
Field of Study	Physics
Thesis Advisor	Dr. Rattachat Mongkolnavin
Thesis Co-advisor	Professor. Chiow San Wong

Accepted by the Faculty of Science, Chulalongkorn University in Partial Fulfillment of the Requirements for the Master 's Degree

…….. Dean of Faculty of Science
(Associate Professor Wanchai Phothiphichitr)

THESIS COMMITTEE

…….. Chairman
(Boonchoat Paosawatyanyong, Ph.D)

……..……. Thesis Advisor
(Rattachat Mongkolnavin, Ph.D)

…….. Thesis Co-advisor
(Professor Chiow San Wong)

…….. Member
(Assistant Professor Kiranant Ratanathammapan)

…….. Member
(Somchai Kiatgamolchai, Ph.D)

บทคัดย่อวิทยานิพนธ์

นายดุสิต งามรุ่งโรจน์ : การดัดแปรพลาสมาโฟกัสสำหรับการปรับสภาพผิววัสดุ. (PLASMA FOCUS MODIFICATION FOR MATERIAL SURFACE TREATMENT)
อ. ที่ปรึกษา : อาจารย์ ดร. รัฐชาติ มงคลนาวิน, อ.ที่ปรึกษาร่วม : PROF. CHIOW SAN WONG, 89 หน้า. ISBN 974-17-1449-1

การใช้เครื่องพลาสมาโฟกัสในการทดลองวิทยาศาสตร์เริ่มตั้งแต่ปี พ.ศ. 2503 และเป็นเครื่องมือที่ เหมาะสมในการศึกษาทางด้านพลศาสตร์ และอุณหพลศาสตร์ของพลาสมา และยังสามารถเป็นแหล่ง กำเนิดพลาสมาต่าง ๆ รวมทั้งแหล่งกำเนิดเอกซเรย์ต่อเนื่อง ใช้ศึกษาปฏิกิริยาฟิวชั่น พลาสมาโฟกัส เป็นเครื่องที่สร้างและเร่งพลาสมาไปตามแนวแกนแซด (Z) ด้วยแรงลอเรนท์ เครื่องสามารถผลิตพลาสมา ที่มีความหนาแน่นสูง ($n > 10^{19}$ ต่อลูกบาศก์เซนติเมตร) อุณหภูมิสูง มีช่วงระยะชีวิตสั้นกว่า 100 นาโนวินาที เมื่อเกิดการโฟกัส การเกิดโฟกัสนี้สามารถนำไปเป็นแหล่งกำเนิดนิวตรอน เอกซ์เรย์ ลำไอออน ลำอิเลกตรอน และกระแสพลาสมาได้

ในงานวิจัยนี้พลาสมาโฟกัสขนาด 3 กิโลจูล ถูกสร้างขึ้นและดัดแปรเพื่อสร้างลำไอออน และกระแสพลาสมาที่มีความแน่นอน เพื่อใช้ในการปรับภาพผิวและเคลือบผิววัสดุ สมบัติของพลาสมาที่เกิดจากพลาสมาโฟกัสถูกศึกษา โดยใช้เครื่องมือวัดต่าง ๆ เช่น หัววัดความต่างศักย์สูง โรโกวิสกี้คอยร์ หัววัดสนามแม่เหล็ก และหัววัดค่ากระแสไฟฟ้า ถูกใช้ในการตรวจสอบลักษณะของพลาสมา ผลการวัดครั้งนี้ได้ถูกนำมาเปรียบเทียบกับการจำลองเชิงตัวเลข พบว่ากระแสที่ถูกถ่ายเทของพลาสมามีค่า 136.77 กิโลแอมป์ และความเร็วของแผ่นพลาสมาสามารถสูงถึง 6 ซม.ต่อไมโครวินาที ภายใต้แรงดัน 0.5 mbar ความเร็วเฉลี่ยของกระแสพลาสมามีค่าประมาณ 0.6 ซม.ต่อไมโครวินาที ตามผลที่ได้และรายงานในสิ่งตีพิมพ์ วิธีการดัดแปรหลากหลายแบบได้มีการทดลองอย่างละเอียดเพื่อศึกษาปฏิกิริยาที่เกิดขึ้นกับพลาสมาไนโตรเจนและพลาสมาอาร์กอนที่เกิดขึ้นกับวัสดุ เช่น แก้ว ไทเทเนียม อลูมิเนียม และเหล็ก ซึ่งการเปลี่ยนแปลงที่เกิดขึ้นอาจเป็นไปได้จากความร้อน และการทำลายที่เกิดขึ้นจากกระแสพลาสมา หรือ ไอออน

ภาควิชาฟิสิกส์ ลายมือชื่อนิสิต.....
สาขาวิชาฟิสิกส์ ลายมือชื่ออาจารย์ที่ปรึกษา .....
ปีการศึกษา 2545 ลายมือชื่ออาจารย์ที่ปรึกษาร่วม .....

AN ABSTRACT

4372265223 : MAJOR PHYSICS
KEY WORD: PLASMA FOCUS / SURFACE MODIFICATION / PLASMA DIAGNOSTIC / COATING / PLASMA

DUSIT NGAMRUNGROJ : PLASMA FOCUS MODIFICATION FOR MATERIAL SURFACE TREATMENT. THESIS ADVISOR : DR. RATTACHAT MONGKOLNAVIN, THESIS COADVISOR : PROF. CHIOW SAN WONG, 89 pp. ISBN 974-17-1449-1.

The Plasma Focus Device has been studed since1960. It is an excellent device for studying plasma dynamics and thermodynamics as well as being a rich source for a variety of plasma phenomena including soft x-ray production and plasma nuclear fusion. Plasma focus is a device that generates and accelerates plasma along Z-direction with Lorentz force. It produces a high-density ($n>10^{19}$ cm^{-3}) and high temperature plasma with a short life time of less than 100 ns during "focussing". This "focussing" process can be an intense source of neutron, X-ray radiation, ions beam, electron beam, and plasma jet.

In this research, a 3 kJ plasma focus device was built and modified with an attempt to produce a consistent ion beam and plasma jet for surface modification and coating of materials. The properties of the plasma from the plasma focus were studied. Several diagnostic tools such as high voltage probe, Rogowski coil, magnetic probe, electric probe were used for characterisation. Results from these measurements are compared with a numerical model. It was found that the discharge current of the plasma is 136.77 kA and the speed of the plasma sheath can reach up to 6 cm/μs under 0.5 mbar of pressure. Average speed of the plasma jet was also estimated to be 0.6 cm/μs. Based on these results many reported publications, several areas of modification method are explored. Thorough experiments were carried out to study the effects of Argon and Nitrogen plasma on materials such as glass, Titanium, Aluminum and steel. The major contribution to surface modification process is possibly from a heating effect as well as a bombardment of ions or plasma jet.

Department Physics Student's signature.....
Field of study Physics Advisor's signature.....
Academic year 2002 Co-advisor's signature.....

ACKNOWLEDGEMENT

I would like to dedicate this section to give my specials gratitude to the people who help and support me through my master thesis work. Without anyone of them, it would be impossible for this thesis to be finished.

First of all I would like to express my great thank to my advisor, Dr. Rattachat Mongkolnavin, and my co-advisor Prof. Chiow San Wong, for their support, great understanding and excellent guidance, which make this thesis possible. This thesis work have gone through a lot of problems and difficult time, but they always have a great patient and give suggestions which help me to solve all these problems. I am also grateful to the following people:

Dr. Boonchoat Paosawatyanyong and Assistant Professor Kirannant Ratanathammapan for great understanding and excellent guidance on my experiment.

Mr. Jasbir Sing, for useful suggestions about the circuit problem. Mr. Boonlare Ngotawonchai for support on data and some idea suggestion. Mrs. Aree Limnirandron for some experimental assistance.

All of my friends, Miss Yap Soung Ling, Mr. Low Yoon Kong, Miss Kanitta Hongleartsakul, Mr. Phairat Khamsing Miss Onanong Chaemlek, Miss Sujira Promnimit and other friends, who made the life in Malaysia and Thailand very pleasant and interesting experience for me.

I would like to thank the Scientific and Technological Research Equipment Center Chulalongkorn University for providing data for my results.

Finally, my sincere thank to Dr. Minella Alarcon, UNESCO and AAAPT for supporting this activity, and my family who always believe in me and support me in everyway they can.

CONTENTS

CONTENTS (Cont.)

List of Tables

List of Figures

List of Figures (Cont.)

Page

List of Figures (Cont.)

Page

List of Figures (Cont.)

Page

List of Figures (Cont.)

Page

CHAPTER 1

INTRODUCTION

1.1 Background

In 1983, the development of a simple plasma focus device for developing countries with simple diagnostics had been discussed at the International Center for Theoretical Physics (ICTP) [1]. The plasma focus is an excellent device for studying plasma dynamics and thermodynamics as well as being a rich source for a variety of plasma phenomena including soft x-ray production and plasma nuclear fusion.

The plasma focus device is a cylindrical coaxial tube, which has outer electrodes surrounding an inner electrode pointing in the Z-axis direction. A glass insulator is used to insulate between the inner and the outer electrode. The discharge is triggering through by a spark gap switch.

In 1998-1999, the work on the plasma focus began by a collaboration between Plasma Research Laboratory, University of Malaya, Malaysia and the Plasma Group, Department of Physics, Faculty of Sicence, Chulalongkorn University. At a later stage, the collaboration was extended to Asian African Association for Plasma Training (AAAPT), This research work is partially supported by UNESCO under a postgraduate student exchange programme.

The plasma focus device has several diagnostic tools which are high voltage probe, Rogowski coil, magnetic probe, ion probe etc. The high voltage probe is used to measure the voltage across inner and outers electrode. Rogowski coil is used for the measurement of the input current of the plasma focus device. The speed

of the plasma sheath generated by the plasma focus can be measured by a magnetic probe. An electric probe is used for measuring the characteristic of the ion beam and the plasma jet.

It is believed that the plasma focus can generate plasma and ions [2]. The ions produced are of high energy such that it can be used for modifying material surface. Several methods of material surface processing are deposition, ion implantation, sputtering, coating and bombardment. An example is described by Hong-Xia Zhang et al. [3]. He claimed that a diamond film can be grown on a steel substrate with Al-N interlayer by using high power plasma streams. Chhaya R. Kant et al have also deposited carbon film on glass, silicon and quartz substrates [4]. He used argon ion from a plasma focus to bombard graphite targets. Another interesting example is from B.B. Nayak et al. They coated carbon nitride on a graphite substrate, again, by using a plasma focus [5]. In this case, graphite electrodes were used in conjunction with nitrogen gas. H Kelly et al [6], as well as R. Gupta [7] et al. have also attempted to coat of TiN on the surface of a metallic substrate. They placed titanium inserts at the end of the inner electrode (anode) and generated nitrogen ions from nitrogen gas. TiN was formed when the nitrogen ions hit the electrode. In addition, Z. Werner et al. investigated and presented a principle of operation of high-intensity pulsed ion plasma beam [8]. He discussed in some detail the concept of magnetic insulation and method of high-density plasma generation which are interesting and related to this work.

Furthermore, A. Lepone et al. discussed the role of the nitrogen ion beam from a small plasma focus for thermal processing of an austenitic stainless steel substrate [9]. Bin and other use pulse-ion high energy density of plasma from a small plasma focus on ceramic surface [10]. From this literature survey, one can see that a

plasma focus can be used as a tool for material surface coating and modification. Therefore, it is interesting to explore further possibility of such application.

In particular, for the plasma focus application, attention has been paid on the use of the ion beam generated from the plasma focus for ion implantation process, thermal surface treatment, and ion-assisted coatings on samples located in front of the coaxial electrodes of the device. In one application, a thin film of TiN was coated at room temperature by a plasma focus [11]. Other applications such as, deposition of graphitic, fullerenes and diamond like carbon on different substrates [4], deposition of Cu^+ on polymer at low pressures [12] have been reported.

1.2 Objectives

In this research, the plasma focus device was built and modified with an attempt to produce a consistent ion beam and plasma jet for surface modification and coating of materials. The plasma jet was studied by electric probes operated in ion saturated region while the ion beam was detected by a biased electric probe. An average ion beam energy and the speed of the plasma jet can be estimated from these measurements.

The dynamics of the plasma focus discharge was studied also. Rogowski coil and several magnetic probes were used to measure the total current and the speed of the plasma sheath. Results from these measurements are compared with a numerical model.

In the last part of the research, several areas of modification method based on previously reported work are explored. An attempt were made to coat copper on insulating substrate. The direct nitriding of Titanium by using the plasma focus was also tested. Treated samples were characterised by Scanning Electron Microscope

(SEM) and Energy Dispersive X-Ray Diffraction (EDX) in order to analyse the deposition qualitatively and quantitatively.

1.3 Thesis Layout

This thesis is divided in to five chapters. In this first chapter, the background and the motivation of the research are given. In Chapter 2, the four dynamic phases of the plasma focus device are described. The components required for the plasma focus are discussed in details. Diagnostic techniques used for studying the characteristics of the plasma focus are explained which include a high voltage probe, Rogkowski coil, magnetic probe, and electric probe. Simulation model of the plasma focus dynamics is tested and described in chapter 3. This simulation leads to interesting comparison of results between the model and experiment.

Chapter 4 shows all experimental results with regard to material surface modification. Physical properties of plasma from the plasma focus are used and explored. Conclusion and discussion of results, both the characteristic of the plasma focus and the changes of material surface are presented in Chapter 5. Further works are also suggested, in this chapter.

CHAPTER 2

PLASMA FOCUS DEVICE

In this chapter, the UNU/ICTP (United Nation University / International Center for Theoretical Physics) plasma focus is discussed in detail. The plasma focus system is made up of many sub-systems [13, 14]. Each sub-system has its own function for the operation of the plasma focus. The dynamics of the plasma produced by the plasma focus are also discussed later in this chapter.

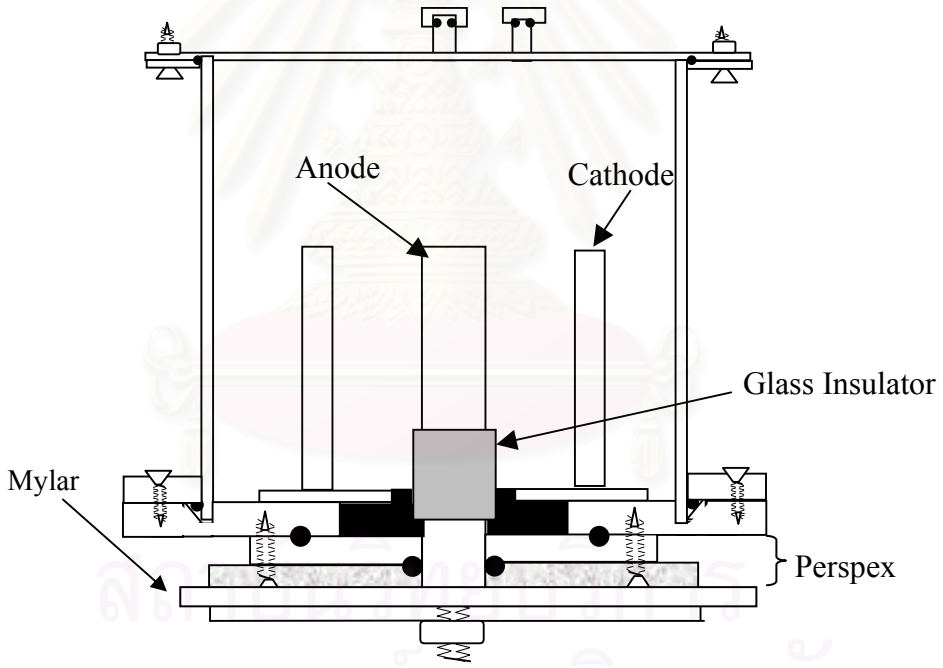

Figure 2.1: A picture showing UNU/ICTP Plasma Focus.

2.1 Plasma Focus Sub-Systems

The UNU/ICTP plasma focus is a small 3 kJ plasma focus which operates at 15 kV (Figure 2.1). It consists of five sub-systems: charge storage, triggering unit and spark gap switch, vacuum pump and a pressure gauge, and plasma

focus tube. An overview of the plasma focus sub-systems is shown as a block diagram in Figure 2.2.

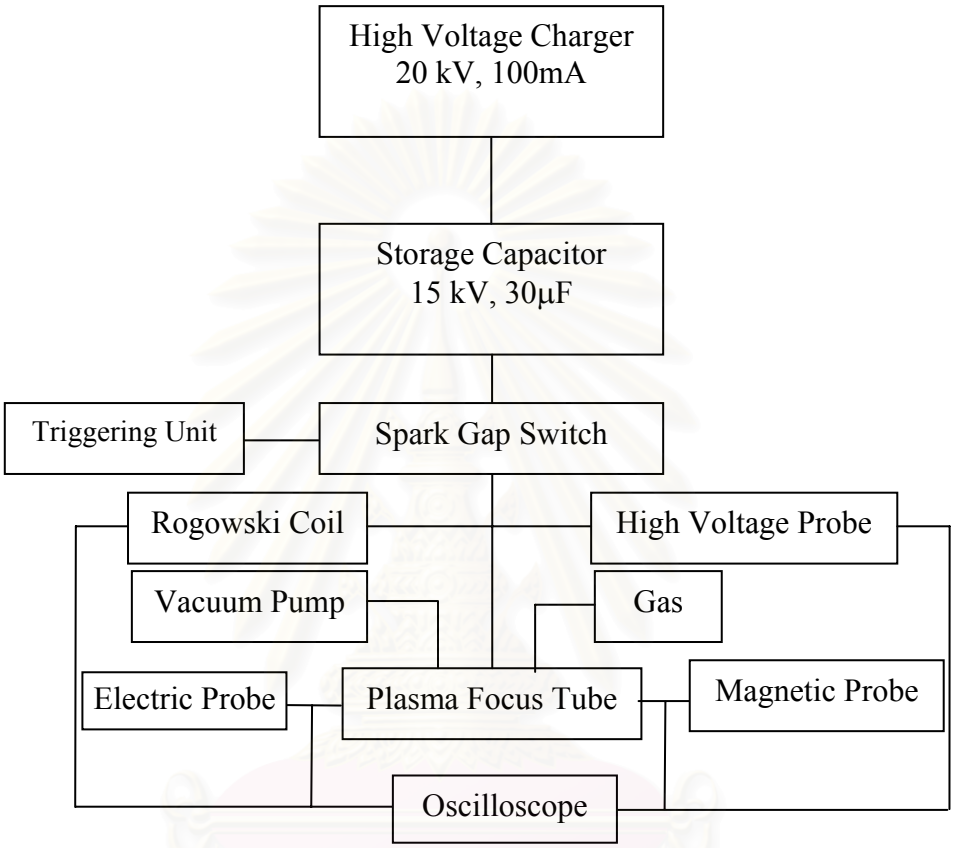

Figure 2.2: A diagram showing an overview of the plasma focus sub-system.

2.1.1 The Storage Capacitor

A special high voltage 30μF 15 kV capacitor is used (APPENDIX D, Figure D1). The capacitor is used to store charges until the potential reaches 12.5 kV when it is discharged and transfer all its electrical energy to the plasma.

2.1.2 The Charging Unit

The charging unit or the charger is used for charging the capacitor through a high voltage resistor (100 kΩ and 100 W). The charger has a maximum

charging voltage of 20 kV. A variac is used for varying the input voltage for a high voltage neon transformer. The neon transformer is used to step up the voltage to 15 kV. A high voltage bridge rectifier changes AC to DC as shown in Figure D2 of Appendix D [15]. The bridge-rectifier is made of many 1N4007 diodes (a 1N4007 can tolerate a maximum voltage of about 300 V). Fifty diodes are linked in series and placed in an insulating Perspex holder filled with transformer oil. Four sets of diode chain are used to make a full wave bridge rectifier. The full wave bridge rectifier is used because its efficiency is much better than the half wave rectifier. The charger circuit is shown in Figure 2.3. A magnetic dump switch is used to short the capacitor to the ground via 100 kΩ resistor in case of accidents.

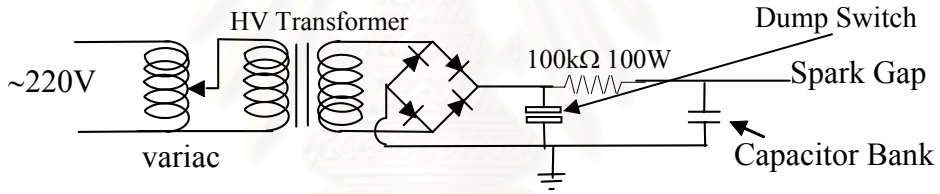

Figure 2.3: A diagram showing the charger circuit.

2.1.3 Triggering Units and Spark Gap Switch

The spark gap switch used in this system (Figure D3 in Appendix D) is a swinging cascade type which operates in atmospheric air. It is controlled by a triggering unit. It is made up of three plates with gaps set at fixed distances. The ratio of the distance between the first and the second plates to the distance between the second and the third plate is 3:2. The first plate is connected to the capacitor. The second plate or the trigger plate is connected to two 50 Ω resistors in parallel, a coaxial cable capacitor and a TV-transformer then to the high voltage triggering unit. The resistors and the capacitor are used to avoid high voltage feedback when the

focus is firing. The third plate or the discharge plate is connected to twenty coaxial cables, which are connected to the anode of the focus tube.

The switching of the spark gap is controlled by a trigger unit. In this set up, an electronic trigger is used. The electronic trigger has two stages; a low voltage SCR unit and a high voltage SCR unit. First, the low voltage SCR unit creates a sharp rising pulse with a peak voltage of ~22 V. This pulse is used to trigger a high voltage SCR unit to give a sharp rising pulse of 800 V. This pulse is then fed through a TV-Transformer which steps up the voltage to 17 times the original voltage. It is connected so that its put is a negative 13.6 kV pulse with 1 μs rise time for the center plate of the spark gap. The circuit of the trigger system is shown in Figure 2.4.

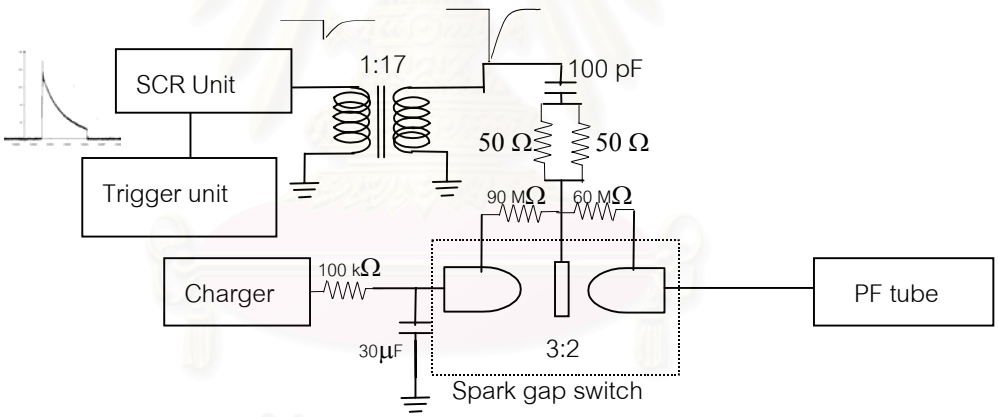

Figure 2.4: A diagram of the spark gap switch used in relation to other sub-system.

2.1.4 Vacuum Pump and Pressure Gauge

Since the operating pressure regime of the plasma focus is not at too low a pressure, the use of a rotary pump is sufficient to produce reasonable vacuum for the chamber of this size. The rotary pump is used to evacuate the plasma tube to a minimum pressure of 10^{-2} torr or 10^{-3} torr (about 0.01333 mbar or 0.0013 mbar [16]). In this project, the operating pressure of between 0.5 mbar to 10 mbar is required.

For vacuum measurement, a standard mechanical pressure gauge is used to display the operating pressure. It is selected as it is more robust and most suitable under this operating condition. This is shown in Figure D4 in Appendix D. The range of pressure that it can measure is between 0.5 mbar to 25 mbar.

2.1.5 Plasma Focus Tube

The plasma focus tube is an important part of a plasma focus device. It has a copper anode at the center. The anode are surrounded by six copper rods each with a length of 16 cm acting as the cathode. In this project, three different anodes are used. A short hollow anode and a short solid anodes, both 16 cm in length, and a long 19 cm hollow anode. Each anode has different functions which will be discussed later in this thesis. The three anodes are the same diameter at 1.9 cm. The cathode rods are arranged in a circle of 6.4 cm diameter.

2.2 Plasma Focus Dynamics

Plasma focus process begins when a charged capacitor bank at a voltage V_o discharges to the plasma focus tube [13, 17]. The high voltage causes a breakdown, initially, on the surface of the glass insulator at the base of the anode. A current sheath (plasma sheath) is formed symmetrically along the electrode axis. It lifts off from the glass insulator and is then propelled by $\vec{J} \times \vec{B}$ force or usually known as Lorentz force. Here, $\vec{J}$ is the current density and $\vec{B}$ is the self-induced magnetic field. This phase is called “breakdown or surface discharge phase” [13] as shown in Figure 2.5a.

Next phase starts when the current sheath lift-off completeds and the current flows radially outward from the inner of anode to the outer cathodes. As this

happens, it builds up a thicker current sheath. When the current sheath is moving out with speed, it will form a shock front in front of the current sheath. The current sheath sweeps up all the charged particles it encounted leaving behind a vacuum immersed in the magnetic field of the current sheath. Between the shock front and the current sheath, the gas is shock heated to a highly ionized state and a plasma slug is formed. Ahead of the shock front, the ambient gas is assumed to be undisturbed. The $\vec{J}\times\vec{B}$ force pushes the current sheath towards the end of the inner electrode along the Z-direction. This phase is call the axial acceleration phase (Figure 2.5b).

When the current sheath reaches the end of the anode, the radial phase starts. During the radial phase the current sheath slides along the surface of the anode in the radial direction by the $\vec{J}\times\vec{B}$ force. The current sheath collapses radially as shown in Figure 2.5c. At the end of the radial phase, a dense plasma column is formed on the axis of the focus tube just off the face of the anode. During this dense plasma phase, soft X-ray and other types of radiations can be emitted from the plasma. This final phase is the focusing phase (Figure 2.5d).

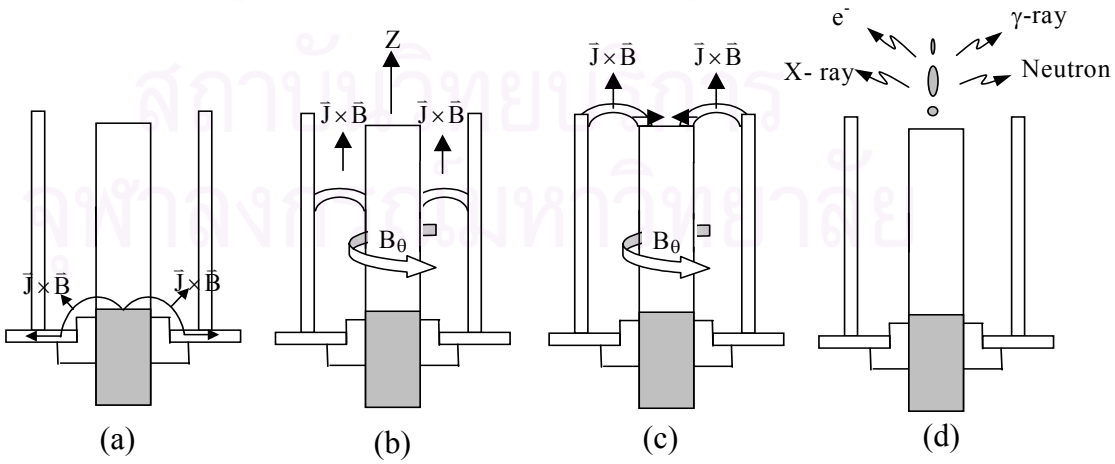

Figure 2.5: Diagrams showing four phases of plasma focus formation: (a) Break down phase, (b) Axial phase, (c) Radial phase and (d) Focusing phase.

2.3 Plasma Jet and Ion Beam

Many researches in the past presented results from experiments which are related to the ion beam and the plasma produced from the plasma focus after the focusing phase. Recently Kazuto Takao and others has done some study on the characteristic of the ion beam produced from a plasma focus [18]. Hétor Kelly et al. used the Faraday cup to detect the nitrogen ion beam generated from a plasma focus device. The plasma focus was operated with pressure at 0.4 torr. The energy of the ion beam was calculated to be about 50 keV.

Z. Werner et al. had done further review of the principles of operation of high intensity pulsed ion and plasma beams [8], E. Yakov et al. presented the energy of the ion beam generated in a plasma opening switch [19]. L.Jakubowski et al. [20] and M. Scholz et al. [21] have observed particle beams and plasma sheath imploding at the end of the anode respectively. The work done at the University of Malaya reported the energy of the ion beam from Argon plasma to be from 200 keV to 400keV [22].

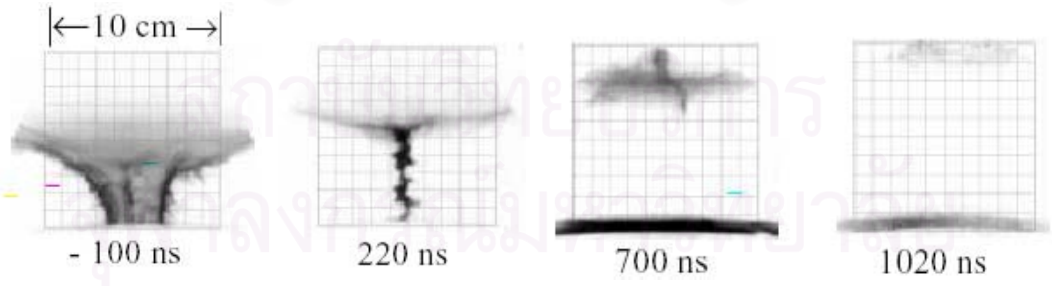

(a) (b) (c) (d)

Figure 2.6: Pictures of pure neon plasma by a fast framing camera: (a, b) obtained during the radial pinching phase and (c, d) during the pinch destruction [23].

The image shown in Figure 2.6 are obtained by V.I.Krauz et al. [23]. These framing images confirm the after event from the focusing. One can see that after the focusing there is a plasma cloud after the breaking up of the plane column by instabilities.

From the literature and the picture above, we believed that after the focusing the high energy ion beam will be formed and then follow by a plasma jet. This hypothesis is shown in Figure 2.7.

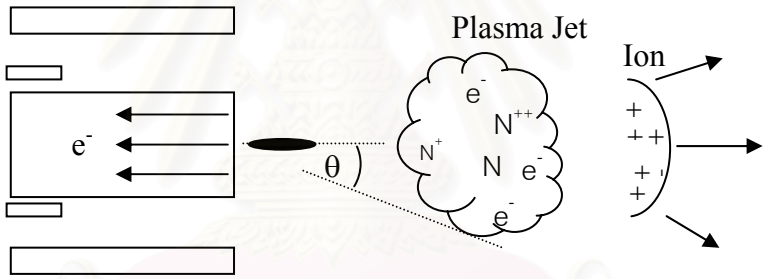

Figure 2.7: A diagram showing a model of ion beam and plasma jet generation by the plasma focus.

Since the plasma jet is much more massive than the ion beam, the velocity of the ion should be much more than that of the plasma jet. In this work, one of the objective is to understand the property of the plasma jet as it may be the dominating source of material surface modification process.

2.4 Plasma Diagnostics

In this project, in order to understand the properties of the small plasma focus, several diagnostic techniques have been used. These include high voltage probe, Rogowski coil [13, 24], magnetic probe [25], and electric probe or ion

probe [24, 26]. These probes are used as tools to measure electrical properties, dynamics, and ion beam. In this section, the details of these probes are discussed.

2.4.1 High Voltage Probe

The voltage measured across the anode and the cathode during the discharge can give a good indication of the focusing process. The high voltage probe is designed to measure this voltage. It is essentially a potential divider. It is mounted across the anode and the cathode at the outer back wall of the discharge tube. This divider essentially consists of 10 pieces of 510 Ω and 1 piece of 51 Ω resistors as shown in Figure 2.8. The signal is measured across the 51 Ω resistor, which is equal to the characteristic impedance of a coaxial cable. The cable is terminated with a matched load of 51 Ω. The signal is recorded via a fast oscilloscope (Tektronik TDS 3034). Essentially the voltage is divided down one hundred times with the high voltage probe. A 10 times attenuator is used to further reduce the signal to a manageable level for the oscilloscope. Figure 2.9 shows the connection of the high voltage probe with respect to the plasma focus device.

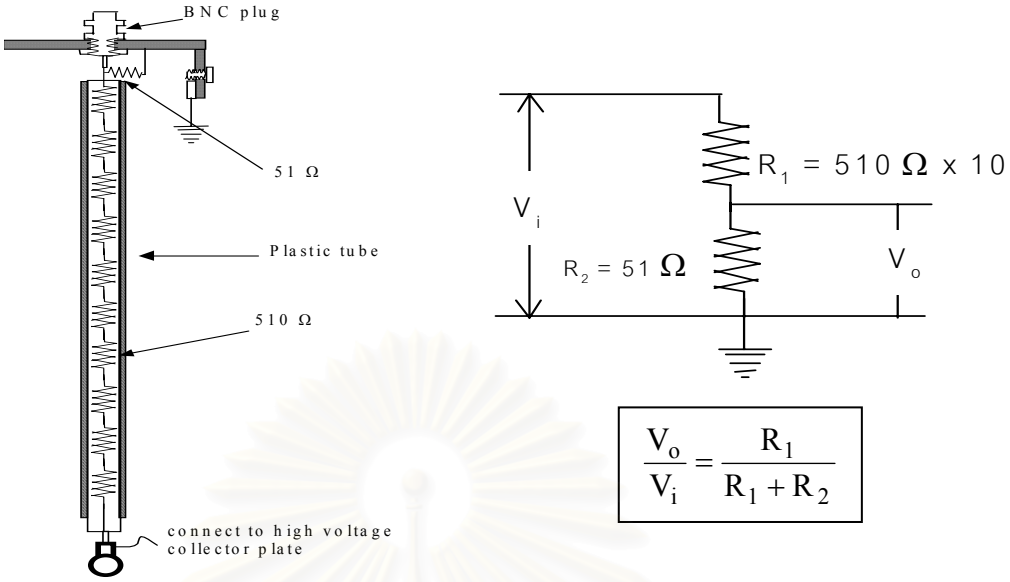

Figure 2.8: A diagram showing the high voltage probe and its equivalent circuit.

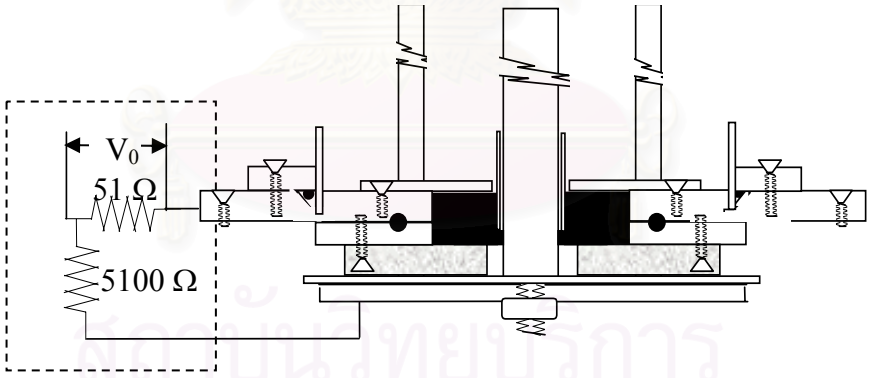

High Voltage Probe

Figure 2.9: A diagram showing the position of the high voltage probe.

2.4.2 Rogowski Coil

During the plasma focus discharge, a very high current is expected to pass through the system in a very short time. The range of the current is between 150 kA to 200 kA. The current can be measured by using a Rogowski coil. The Rogowski coil is essentially a multi-turn solenoid made from copper wire and bent into the shape of a torus as shown in Figure 2.10. The coil is mounted around the anode as shown in Figure 2.11. It is used to indirectly measure the main discharge current by mean of magnetic induction. The signal produced is again measured by the fast oscilloscope.

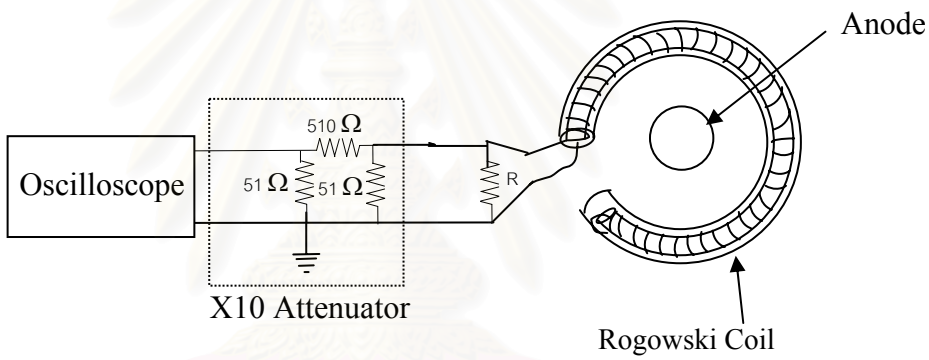

Figure 2.10: A diagram showing the Rogowski coil and its equivalent circuit.

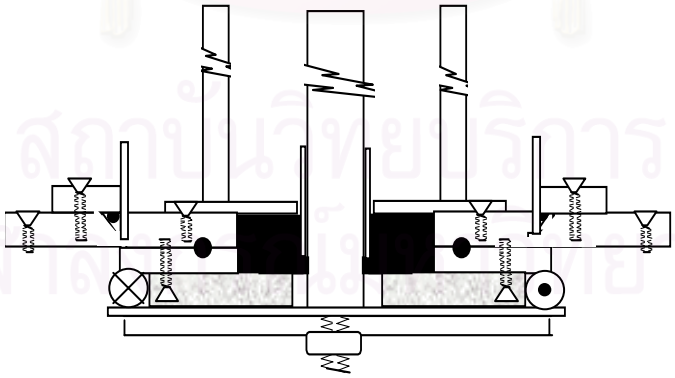

Figure 2.11: A diagram shows the placement of the Rogowski coil with respect to the plasma focus.

The sensitivity of the coil can be calibrated by using a lightly damp sinusoidal L-C-R discharge circuit [13] as shown in Figure 2.12. A typical signal recorded from a plasma focus discharge is shown in Figure 2.13.

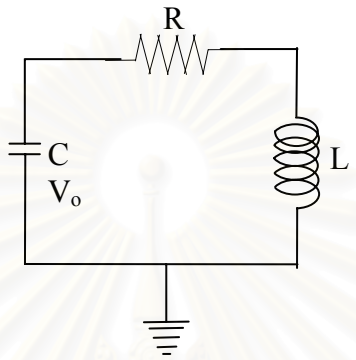

Figure 2.12: A diagram showing the LCR discharge circuit.

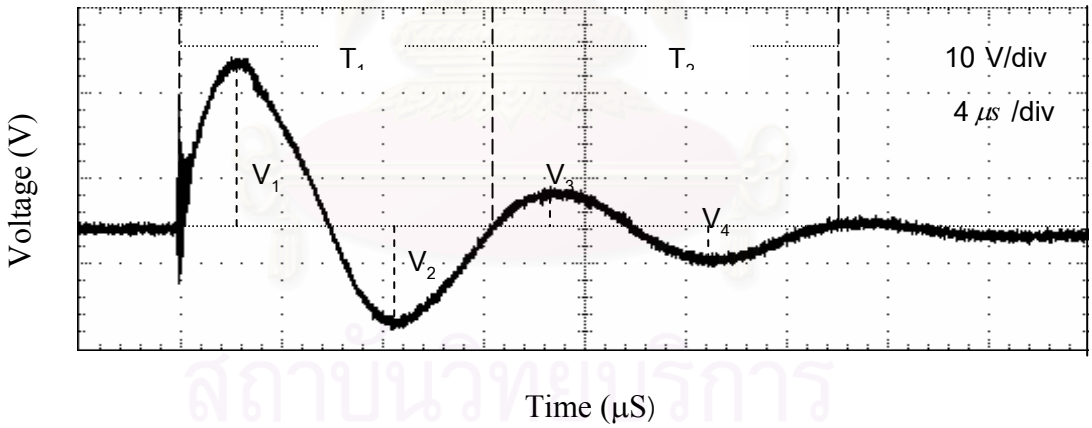

Figure 2.13: Signal from Rogowski coil of a nitrogen plasma at a pressure 3 mbar.

From the equivalent circuit of a Rogkowski coil, it can be shown that the first peak of the discharge current, I_o, can be determined from the following expression:

$$I_o = \frac{\pi C_o V_o (1+f)}{T} \qquad (2.1)$$

Where f = reversal ratio of the current = $\frac{1}{3}(\frac{v_2}{v_1} + \frac{v_3}{v_2} + \frac{v_4}{v_3})$

C_o = capacitance of the capacitor.

V_o = the initial charging voltage

T = the periodic time of the current waveform

By knowing the calculated I_o and the amplitude of the first peak of the current waveform, $V_{o,}$ measured from the oscilloscope, the calibration factor or the sensitivity of the coil can be defined as:

$$K = \frac{I_o}{V_o} \qquad (2.2)$$

2.4.3 Magnetic Probe

The magnetic probe is a similar diagnostic device as the Rogkowski coil [16, 17]. Both work on the same principle of magnetic induction. In this case, a small coil is used. The coil has a thirty turns of copper wire with a diameter of 0.1 mm. The small coil is made and placed into a small glass tube. The glass tube is inserted between the anode and cathode through the top plate of the chamber. The coil is oriented in such a way that it is orthogonal to the magnetic field for maximum current induction.

The magnetic probe is also connected to a simple integration network shown in Figure 2.14, together with a 51 Ω resistor in order to integrate the charge

induced. The resistor is required as it is used for terminating the end of the transmission line leading from the probe.

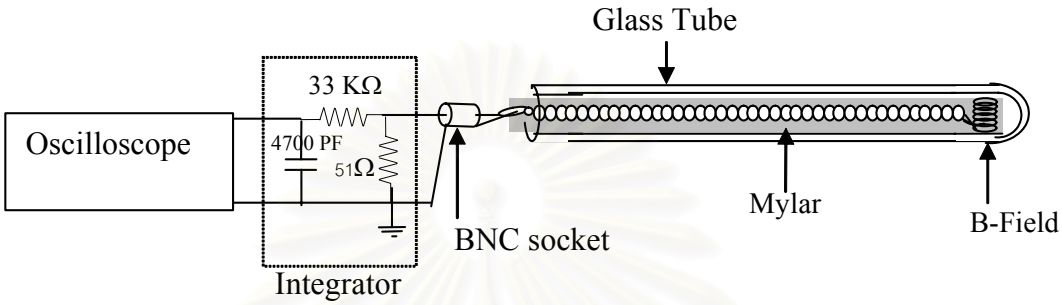

Figure 2.14: A diagram showing a magnetic probe and an integrating circuit.

In this research, the magnetic probe is adapted and used for measuring current sheath velocities. By having a number of coils at a known fixed distance apart (Δs), one can deduce the velocity of a moving current sheath by a time of flight (Δt) method. As the current sheath is passing the coil there will be a rise in signal. This rising of signal marks the time of the current sheath passing through the coil, therefore with two coil at Δs apart the velocity v is;

$$v = \frac{\Delta s}{\Delta t}. \qquad (2.3)$$

A typical signal from the magnetic probe is shown in Figure 2.15

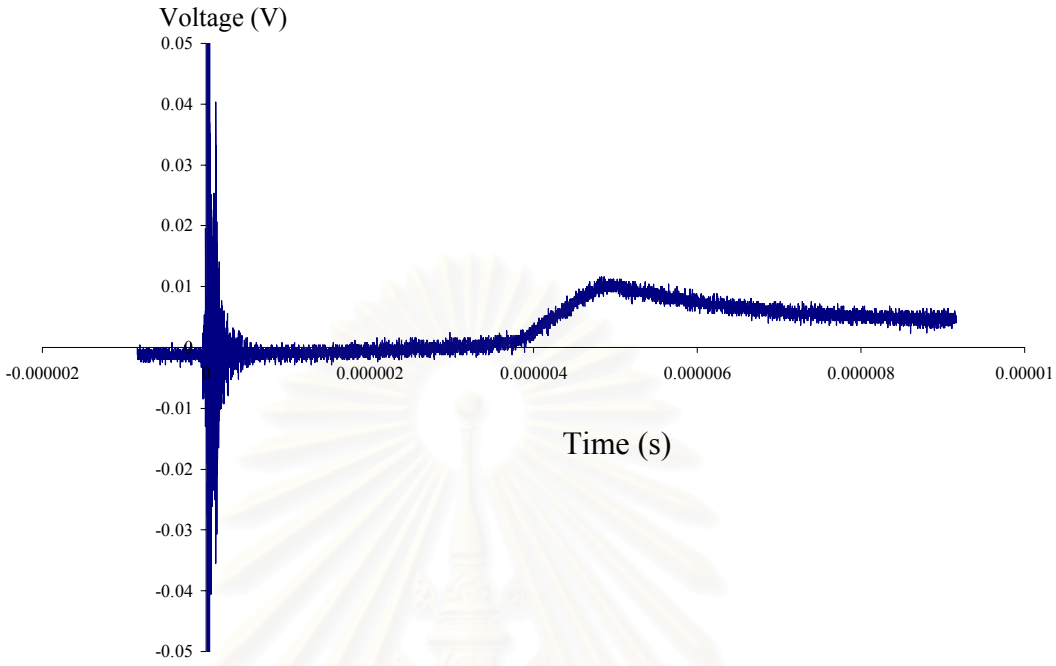

Figure 2.15: A graph showing a signal of the magnetic field detected by the magnetic probe during the plasma focus discharge with 3 mbar of Nitrogen gas.

2.4.4 The Electric Probe

One of the fundamental techniques for measuring the properties of plasma is by using electric probes. This technique was developed by Langmuir in 1924. The electric probe is sometime known as Langmuir probe [13].

An electric probe is a small-insulated wire inserted in the plasma focus tube for detecting electrons or ions of plasma jets. The probe is attached to the power supply capable of biasing at various voltages, positive or negative relative to the plasma (the circuit is shown in Figure 2.16), and the current collected by the probe then provides information about the condition of the plasma. Due to the difference in potential between the probe and the plasma (V_p), charge can flow around the probe circuit thus constituting the probe current I_P.

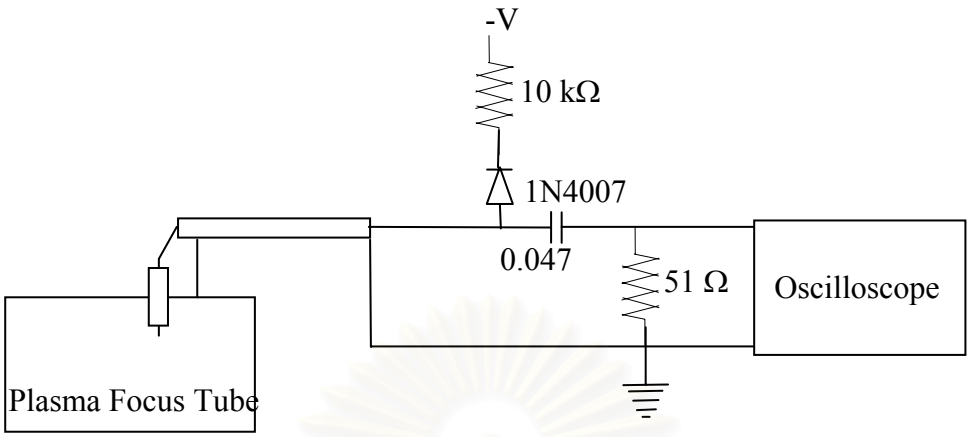

Figure 2.16: A diagram showing an electric probe and its circuit.

For the characteristic of electric probe, the variation of I_p with V_p is related to the plasma parameters such as the electron temperature and electron density. A general the probe characteristics is shown in Figure 2.17.

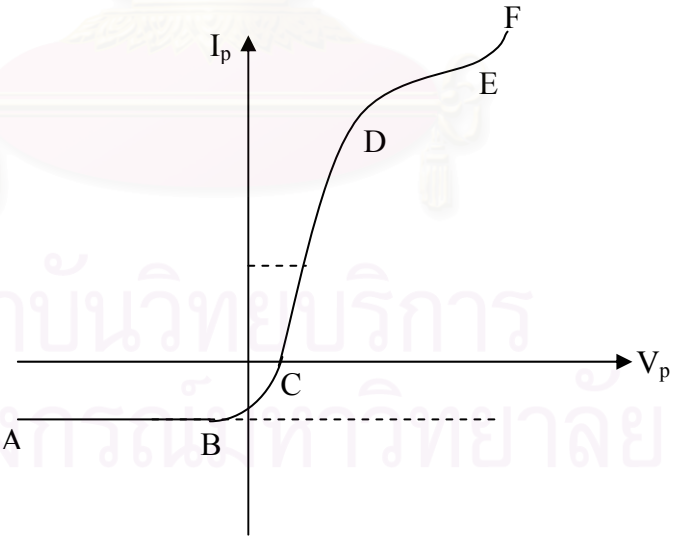

Figure 2.17: A graph showing a relationship between current and voltage which indicates general characteristic of the electric probe.

In region AB in Figure 2.17, the probe potential is sufficiently negative where only the ions can reach the probe surface. Next, by start at point B the number of electrons increases and found to be able to reach the probe surface thus reduce the value of I_p, until reaching the point C. Between point C and point D, the electrons reach the surface of the probe, hence linearly increasing the electron current. At point C the probe potential is switch over to positive because the number of ions and electron reach the probe is equal, thus Ip become zero. At point D, the plasma potential is exactly balanced by the probe potential. In region DE the probe surface is effect by thermal motion only. In region EF, the electrons are accelerated when traversing through to the probe. The energies of these accelerated electrons may not be enough to induce secondary ionization through collision, until V_p is increased.

In this thesis two mode of operation of electric probe were studies. In the first mode, a solid coaxial cable diameter with 0.48 cm is put in a small glass tube (0.5 cm) as shown in Figure 2.18. The probe is connected directly to a coaxial cable and to the fast oscilloscope via a bias circuit.

In the second mode, only the bare center conducting wire of a coaxial cable is used. It is put in a plasma focus tube with an insulating cover as shown in Figure 2.19. The center conducting wire is connected directly of to a BNC plug supported by the plastic plate. A 50Ω terminator is connected between BNC plug and the oscilloscope.

In this project, both model are used. The positions of the probes are adjusted in order to measure the velocity of ion beam or the plasma jet by the time of flight technique.

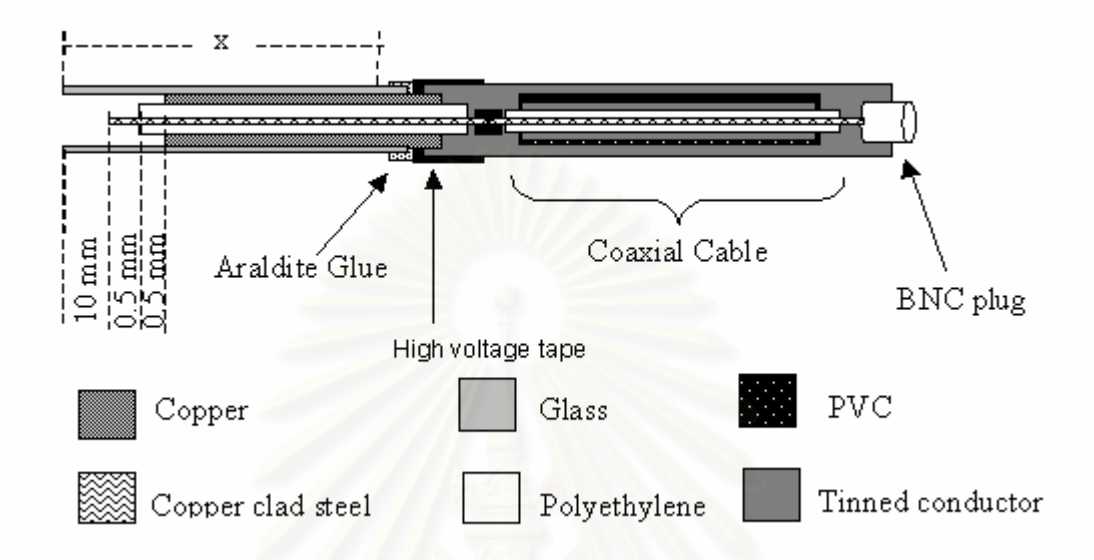

Figure 2.18: A diagram showing an electric probe (Type I).

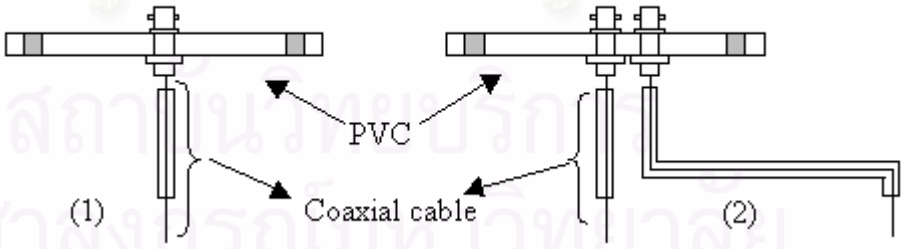

Figure 2.19: A diagram showing an electric probe (Type II).

CHAPTER 3

EXPERIMENT AND RESULT

In this chapter, experiments and results from the plasma focus are described. A 3 kJ plasma focus device (UNU/ICTP PFF) as described in Chapter 2 was built. The diagnostics described were used in a series of experiment to determine characteristics of the plasma focus. A simulation of the axial phase has also been attempted. The detail is stressed on the axial phase, as it is believed to be the crucial phase for material processing investigation. The main characteristics of the plasma focus are voltage, current, velocity of plasma sheath, and velocity of the plasma jet. A summary of the scope of experiments is shown in Figure 3.1.

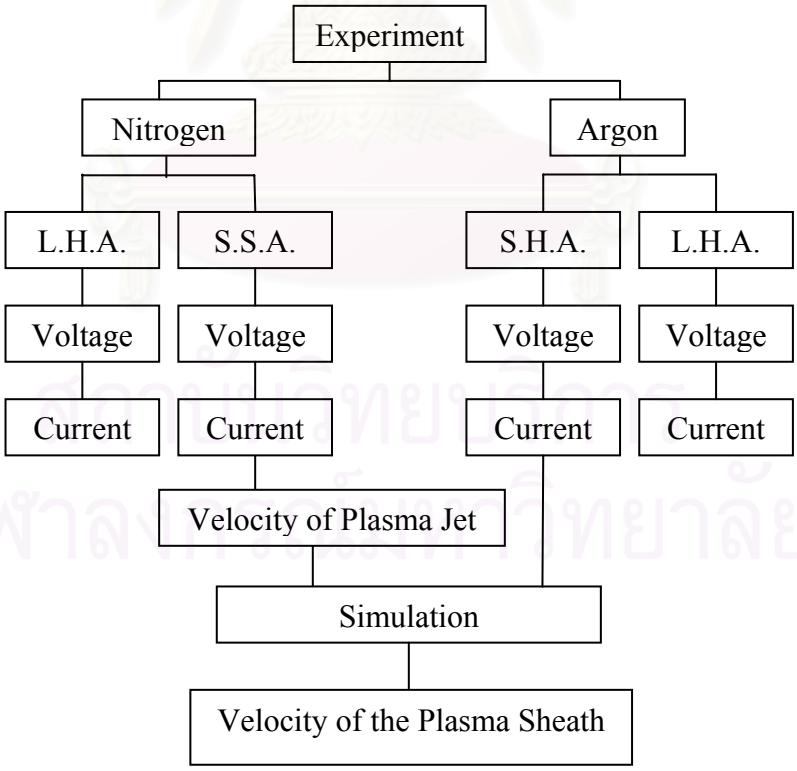

L.A.= Long Hollow Anode: S.S.A= Short Solid Anode: S.H.A= Short Hollow Anode

Figure 3.1: A schematic showing overview of experiments carried out in this research.

In a normal operating condition, the plasma focus is operated when the 30 μF capacitor bank is charged to 12.5 kV. The discharge energy can be estimated to be about 2.2 kJ per shot. Argon or Nitrogen are used as the filling gas. When the focus is fired the data from the high voltage probe, the Rogowski coil, magnetic probe, five channels PIN-diode and electric probe (ion probe) are recorded simultaneously. The oscilloscope used has four channels therefore a combination of measurement is decided before each shot. Normally the signal from the high voltage is used as the trigger signal.

3.1 Voltage and Current Signal Measurement

The voltage and current signal measurements are two basic and fundamental measurements for the plasma focus characteristics.

3.1.1 Voltage Measurement

One can use the voltage characteristics to show the four phases of the plasma focus as described in Chapter 2. A typical voltage signal measured by the high voltage probe is shown in Figure 3.2.

From the voltage signal in Figure 3.2, Peak A indicates the breakdown phase where plasma is beginning to form. The voltage measured from the oscilloscope is 7.28 V which means the actual voltage is 7.28 x 1000 = 7.28 kV. Peak B shows the dense plasma phase. At this time the plasma is at a highest density. The voltage of this peak is 11.87 V x 1000 V = 11.87 kV. Between peak A and peak B the time for axial phase and radial phase is measured to be 3.544 μs. Since we know that the length of the anode is 16 cm, which is the length for the plasma sheath to travel

before focusing, We can deduce the average speed of the plasma sheath to be 16cm/3.544 μs = 4.514 cm/μs.

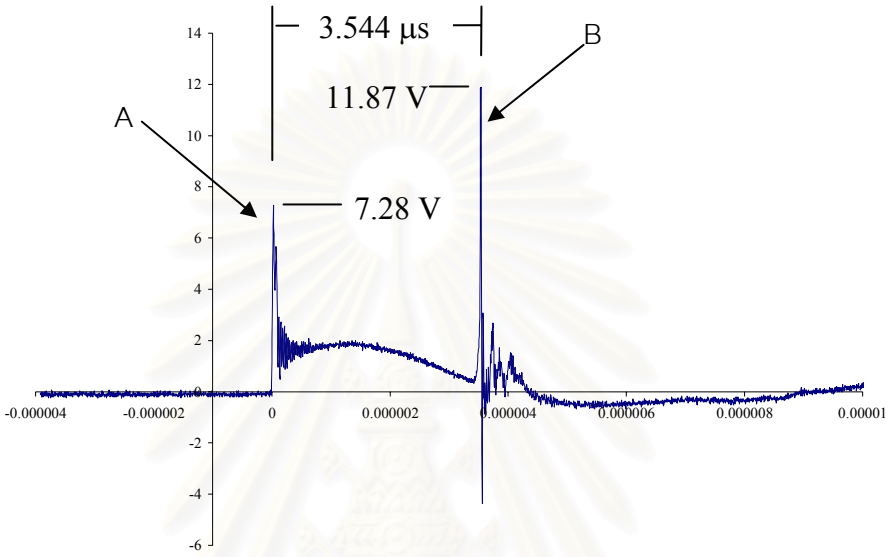

Figure 3.2 : A graph showing a typical voltage signal measured from the plasma focus operating with 0.5 mbar filling gas pressure. The signal has a high voltage peak which indicates the focusing phase.

3.1.2 Current Measurement

In order to find out the value of the peak current of the plasma focus one needs to recalibrate the scale of the oscilloscope. A current factor K must be calculated. A current signal at high operating pressure is used in order to conform to the calculation. By measuring the current signal at a high pressure, a sinusoidal current signal is registered.

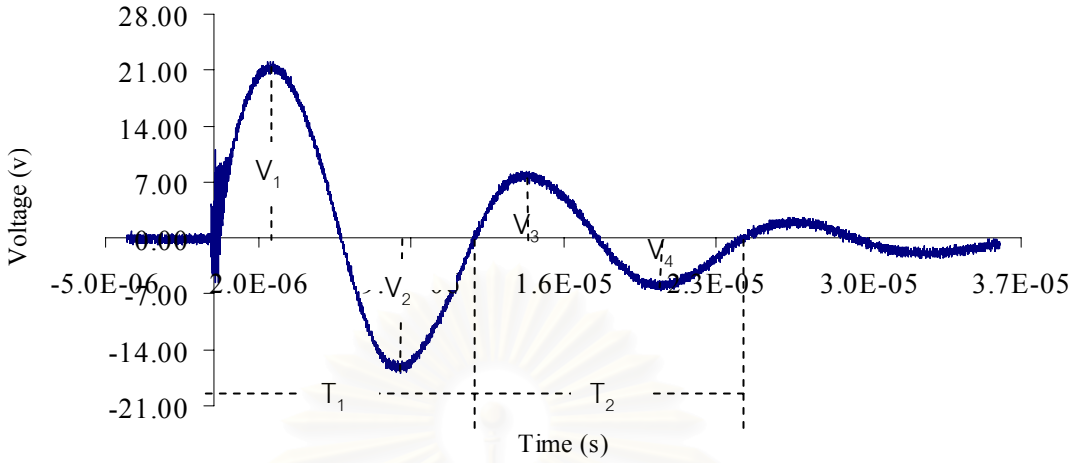

Figure 3.3 : A graph showing a typical current signal detected by the Rogowski coil from the plasma focus with 7 mbar of argon gas and a charging voltage of 12.5 kV.

From Equation 2.1 in Chapter 2,

$$I_1 = \frac{\pi C_o V_o (1 + f)}{T}$$

$$T = \frac{T_1 + T_2}{2}$$

and,

$$K = \frac{I_1}{V_1}.$$

For $T_1 = 12.1$ μs and $T_2 = 12.35$ μs (from Figure 3.3),

$C_o = 30$ μF,

$V_o = 12.5$ kV,

$V_1 = 21.8$ V, $V_2 = 16.4$ V, $V_3 = 8.2$ V, $V_4 = 5.8$ V,

we have,

$$T = \frac{12.1 + 12.35}{2} = 12.28 \text{ μs}$$

$$f = \frac{1}{3}\left(\frac{16.4}{21.8} + \frac{8.2}{16.4} + \frac{5.8}{8.2}\right) = 0.653$$

$$I_o = \frac{\pi \times 30 \times 10^{-6} \times 12.5 \times 10^{3} \times (1 + 0.653)}{12.28 \times 10^{-6}}$$
$$= 158.602 \text{ kA}$$

therefore,

$$K = \frac{158.602 \times 10^{3}}{21.8}$$
$$= 7.275 \text{ kA/V}$$

The maximum current for the plasma focus signal showing in Figure 3.3 is 136.77 kA, where the maximum current V_1 is 18.8 V.

3.1.3 Variation of Voltage and Current Signal Under Different Pressure.

In this section, it is interesting to investigate the changes of voltage and current signals under different operating pressures. An optimum focusing condition can be determined from this experiment. It is important to know these conditions as these will aid the determination of the deposition or material surface modification processes. Which will be discussed in Chapter 5.

The results in Figure 3.4 show sets of voltage and current signals measured from the plasma focus operating under different pressures; 0.5, 1.0, 1.5, 2.0, 2.5 and 3.0 mbar; of argon gas. The time difference between peak A and peak B is measured (Figure 3.2). For the voltage signals, there are differences in the time measured for the current sheath to move to the end of the anode. Since the length of the anode is fixed at 16 cm, we can see that the average velocities of the plasma sheath at different pressure changes. If the pressure is high then the average velocities

is lower. This result is expected. It is also interesting to note that the focus peak is weaker as the pressure is higher. The results are summarized in Table 3.1.

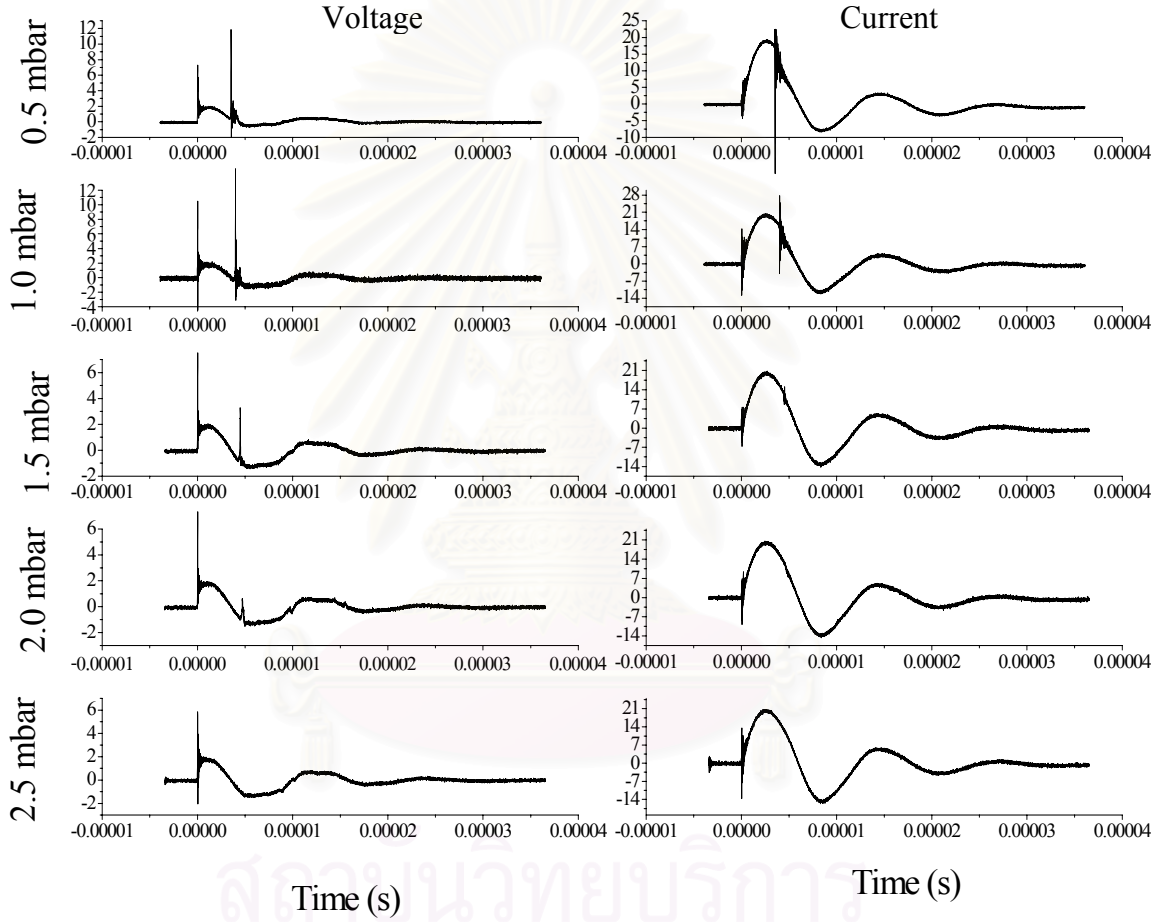

Figure 3.4: A series of graphs showing voltage and current signals from the plasma focus operated with argon and short hollow anode for pressure between 0.5 mbar to 2.5 mbar

Pressure (mbar)	Time average (peak A to peak B (Figure 3.2)) (μs)	Average velocity (cm/μs)	Voltage in focusing peak (V)
0.5	3.4136	4.69	11.8637
1	3.9520	4.05	10.4789
1.5	4.3416	3.69	3.2812
2.0	4.8000	3.33	0.6000

Table 3.1: A table showing the variation of average velocity and the peak focusing voltage at different pressures.

Form Table 3.1 we can see that for the operating pressure between 0.5 mbar to 2 mbar the plasma is focused and the focusing voltage is higher for the high pressure and gradually decreasing as the pressure decreases. The relationship of the peak voltage and the pressure is shown in Figure 3.5. At a pressure greater than 2 mbar we are unable to obtain the focusing peak signal. The time for focusing from the beginning of the discharge (time between peak A and peak B) increases when higher pressure. Because of the increase in time, the average velocity of the plasma sheath is inversely proportional to the pressure. The result is shown in Figure 3.6.

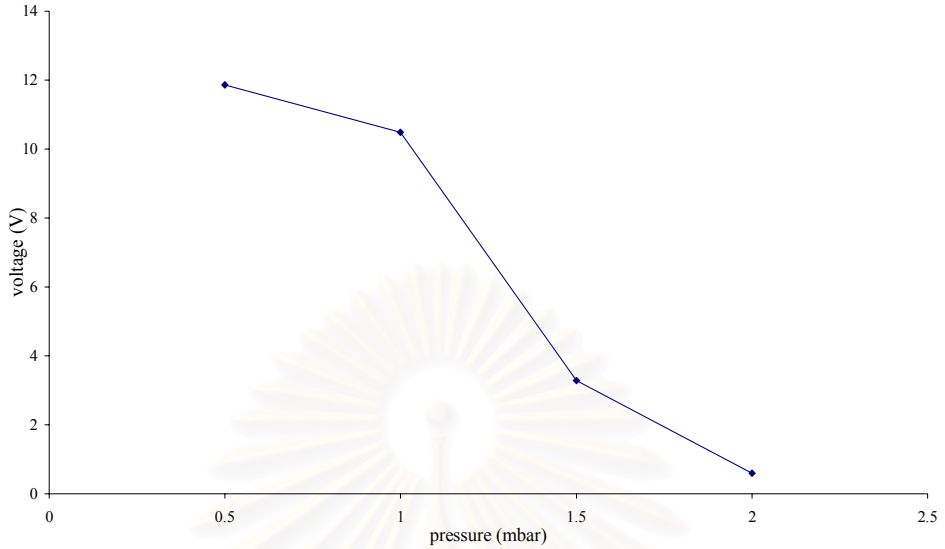

Figure 3.5: A graph showing a relationship between pressure and the peak focusing voltage for the plasma focus operated with argon gas and short hollow anode.

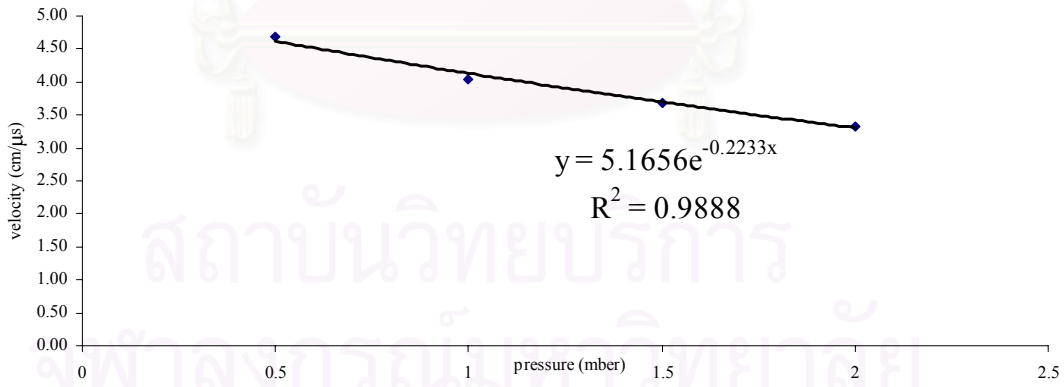

Figure 3.6: A graph showing a relationship between pressure and the velocity for the plasma focus operated with argon gas and short hollow anode.

3.1.4 Measurement of Voltage and Current Signal of Different Plasma.

In this experiment, different filling gases are used in order to generate different plasmas. Argon gas and Nitrogen gas are used as test gases. The same experimental procedure as described in previous section was used to measure the current and voltage signal. A comparison of voltage and current signal from nitrogen gas and argon gas is shown in Figure 3.4 and Figure 3.7 respectively. Table 3.2 and Table 3.3 also show a comparison data of the two.

Pressure (mbar)	Peak focusing signal			
	Argon gas		Nitrogen gas	
	signal	V-peak (V)	signal	V-peak (V)
0.5	focus	11.8637	focus	7.725
1	focus	10.4789	focus	7.520
1.5	focus	3.2812	focus	5.231
2	focus	0.6000	focus	4.800
2.5	Non-focus	-	focus	0.800
3	Non-focus	-	Non-focus	-

Table 3.2: A table showing a comparison of the peak voltage between Argon and Nitrogen gas.

Pressure (mbar)	Time average (peak A to peak B figure 4.2) (μs)		Average velocity (cm/μs)	
	Ar	N_2	Ar	N_2
0.5	3.1136	3.1960	4.69	5.01
1	3.9520	3.4552	4.05	4.63
1.5	4.3416	3.8392	3.69	4.17
2.0	4.8000	4.1904	3.33	3.82
2.5	-	4.5664	-	3.50

Table 3.3: A table showing the variation of average velocity at different pressures for Argon and Nitrogen gas.

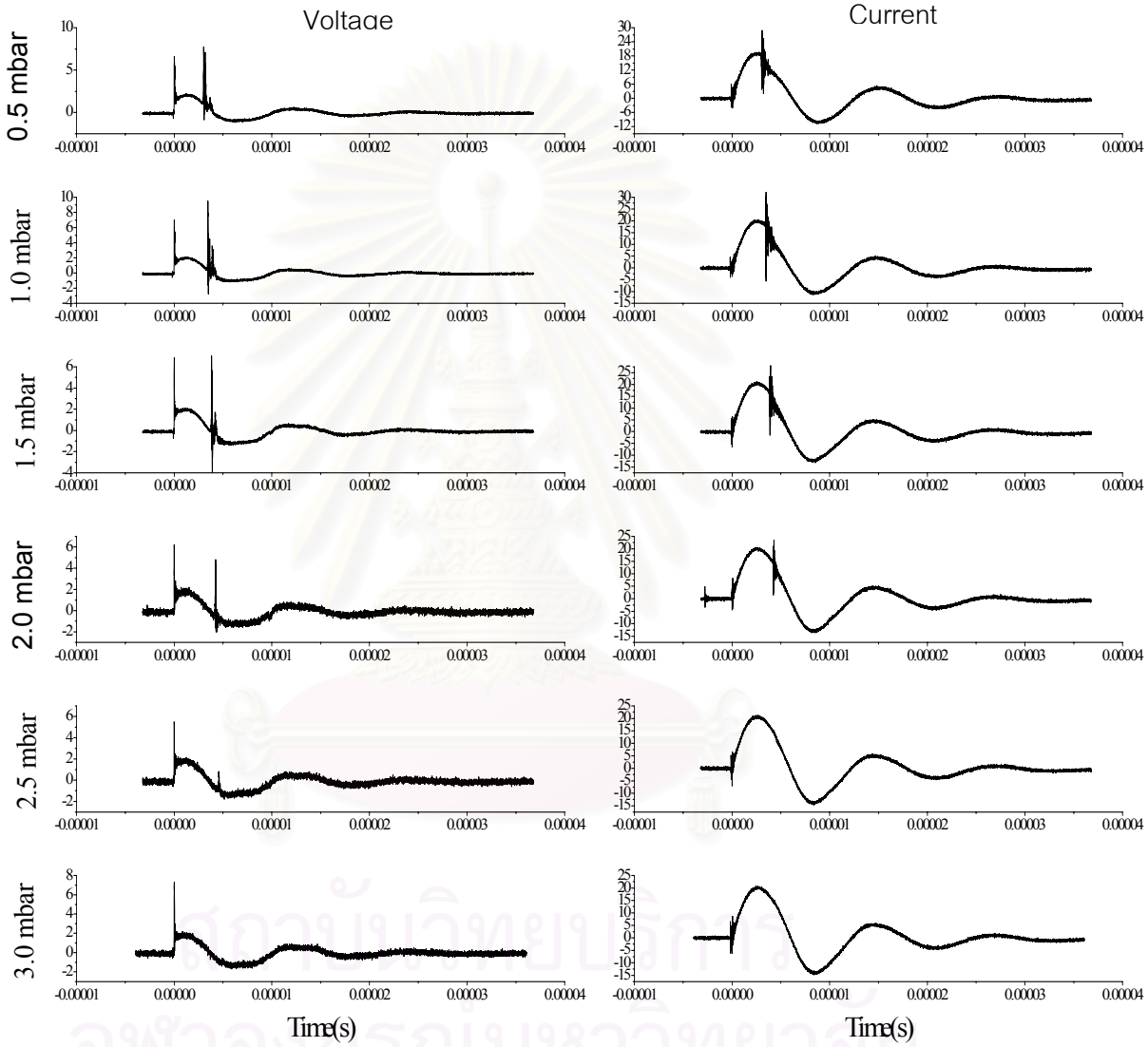

Figure 3.7: A series of graphs showing voltage and current signals from the plasma focus operated with Nitrogen and short solid anode for pressure between 0.5 mbar to 3.0 mbar.

Measurement of voltage and current signal were also made for a special case of longer anode, with a length of 19 cm. The objective of this experiment is to see whether the anode configuration will have an effect on the focusing process. For some surface modification of material, one may not need the focusing process, therefore it is interesting to explore all possibilities and ways to suppress the focusing in a lower pressure regime.

Result of a longer anode length with argon as a filling gas is shown in Figure 3.8. A comparison of the peak voltage is also shown in Table 3.4.

Pressure (mbar)	Peak Focusing signal			
	Long anode		Short anode	
	signal	V-peak(V)	signal	V-peak(V)
0.5	focus	6.88	focus	11.8637
1	focus	6.19	focus	10.4789
1.5	focus	3.519	focus	3.2812
2	Non-focus	-	focus	0.6000
2.5	Non-focus	-	Non-focus	-
3	Non-focus	-	Non-focus	-

Table 3.4: A table showing a comparison of peak voltage for long anode (19 cm) and short anode (16 cm).

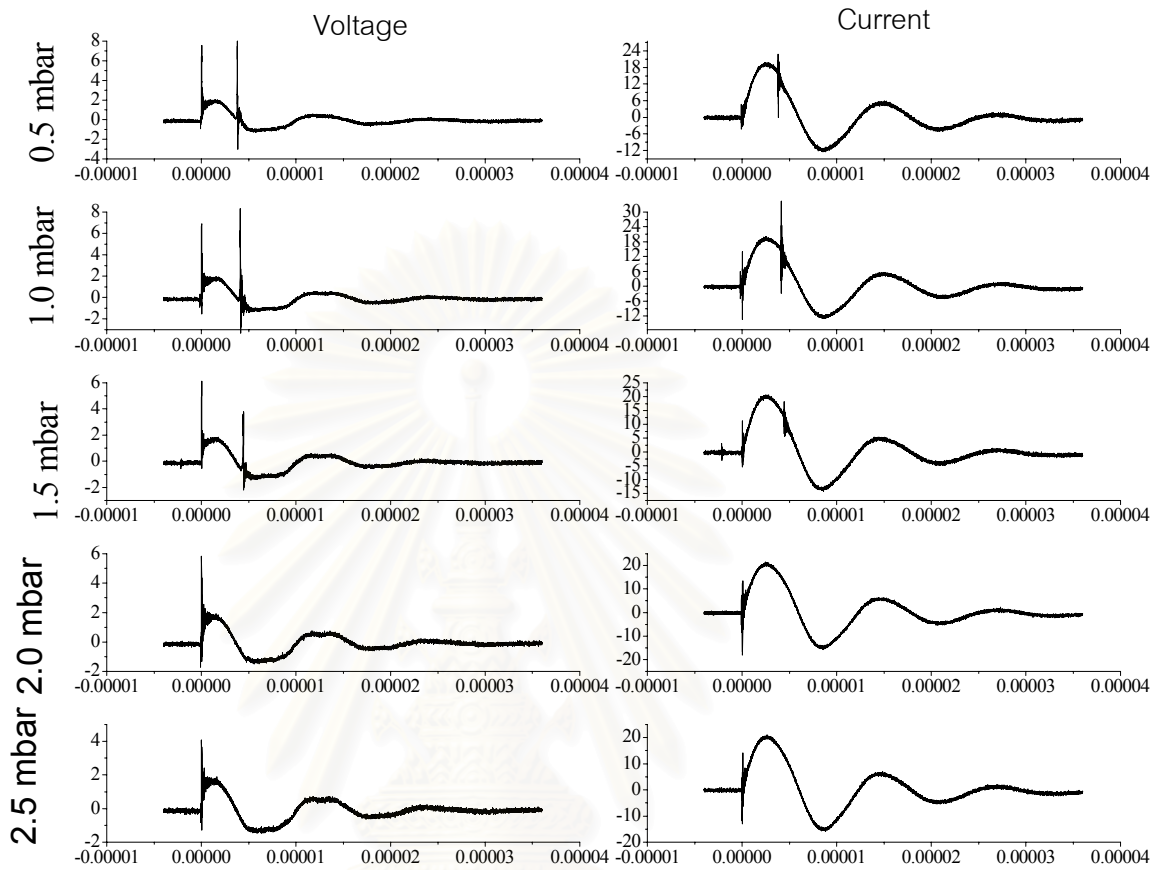

Figure 3.8: A series of graphs showing voltage and current signals from the plasma focus operated with Argon and long hollow anode for pressure between 0.5 mbar to 2.5 mbar.

3.2 Simulation Model

The simulation model for the axial phase of a plasma focus uses 1-dimensional Slug Model. We assume that the current sheath acts as a piston and moving along z-axis between the anode and cathodes as shown in Figure 3.9. If the current sheath is moving at a great speed then there will be an associated shock front in front of the current.

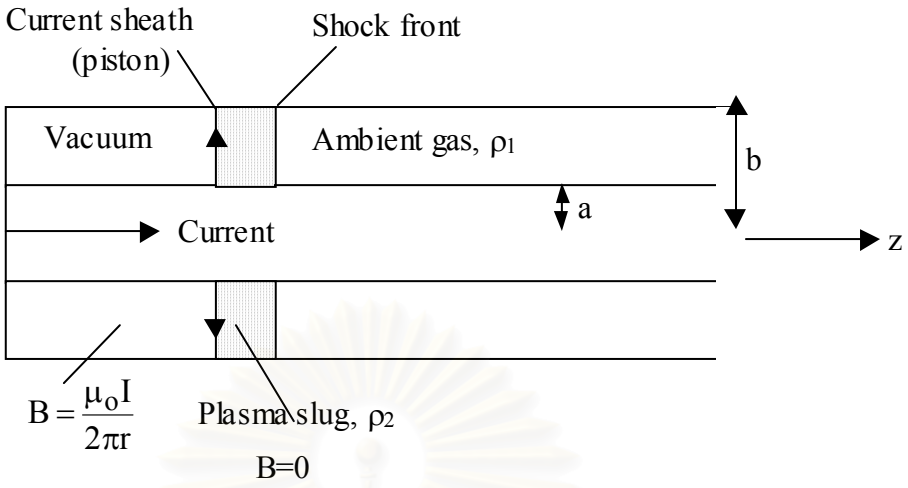

Figure 3.9: A diagram showing a slug model used for numerical modeling of axial phase.

Where ρ_1 = density of ambient gas,

ρ_2 = density of plasma slug,

a = radius of anode,

b = radius of around cathode,

z = shock front position,

B = magnetic field,

μ = permeability.

3.2.1 Equation of Motion

An equation of motion for the current sheath in axial phase can be written as the rate of change of momentum which equates to the Lornetz Force. The equation of motion is shown in equation 3.1.

$$\frac{d}{dt}\left[\rho_1\pi\left(b^2-a^2\right)z\left(\frac{\Gamma-1}{\Gamma}\frac{dz}{dt}\right)\right]=\int_a^b\frac{B^2}{2\mu}2\pi r dr \qquad (3.1)$$

Where

$\Gamma = \frac{\rho_2}{\rho_1}$: mass ratio,

$\rho_1 \pi\left(b^2 - a^2\right)$: mass in slug,

$\left(\frac{\Gamma - 1}{\Gamma}\frac{dz}{dt}\right)$: speed of piston,

$\frac{dz}{dt}$: shock speed,

$\frac{B^2}{2\mu_o}$: magnetic pressure,

$\int_a^b \frac{B^2}{2\mu} 2\pi r dr$: $\vec{J} \times \vec{B}$ Lorentz Force.

From the equation of motion (Equation 3.1), the acceleration of the piston (current sheath) is,

$$\frac{d^2z}{dt^2} = \frac{\frac{\mu_o}{4\pi^2\rho_1}\left[\frac{\ln(b/a)}{b^2 - a^2}\right]\left(\frac{\Gamma}{\Gamma - 1}\right)I^2 - \left(\frac{dz}{dt}\right)^2}{z}. \qquad (3.2)$$

The rate of change of current per unit time can be written from an equivalent circuit equation of a discharging plasma focus using Kirchoff's law as shown in Figure 3.10.

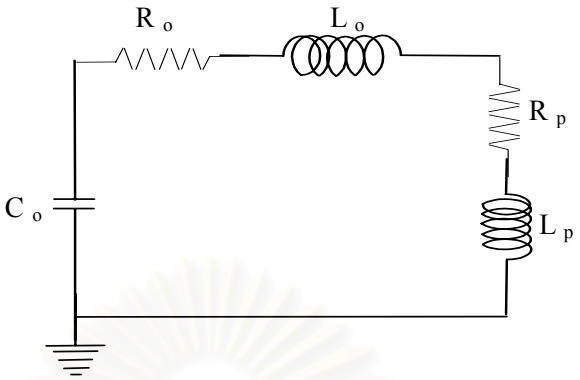

Figure 3.10: An equivalent circuit diagram of a small plasma focus.

From this equivalent circuit, the circuit equation of the axial phase can be written from the sum of voltages around a close circuit loop;

$$\frac{d}{dt}[(L_o + L_p I)] + I(r_o + r_p) = V_o - \frac{\int_0^t Idt}{C_o}.$$

Where L_p is the plasma inductance which can be expressed as:

$$L_p = \frac{\mu_o}{2\pi}\frac{\Gamma - 1}{\Gamma}\ln(\frac{b}{a})z.$$

By assuming,

$$\frac{d}{dt}[(L_o + L_p I)] >> I(r_o + r_p),$$

we can get an expression for the rate of change of current to be,

$$\frac{dI}{dt} = \frac{V_o - \frac{\int Idt}{C_o} - \frac{\mu_o}{2\pi}(\frac{\Gamma - 1}{\Gamma})\ln(\frac{b}{a})I\frac{dz}{dt}}{L_o + \frac{\mu_o}{2\pi}(\frac{\Gamma - 1}{\Gamma})\ln(\frac{b}{a})z} \qquad (3.3)$$

By coupling the circuit equation (Equation 3.3) and the equation of motion (Equation 3.2) together and using normalisation method, the equations can be written as,

$$\frac{d^2\zeta}{d\tau^2} = \frac{\alpha^2\iota^2 - (\frac{d\zeta}{d\tau})^2}{\zeta}, \tag{3.4}$$

and,
$$\frac{d\iota}{d\tau} = \frac{1 - \int \iota d\tau - \iota\beta \frac{d\zeta}{d\tau}}{1 + \beta\zeta} \tag{3.5}$$

Where the normalization factors are;

$$\zeta = \frac{z}{z_0}, \tau = \frac{t}{t_0}, \iota = \frac{I}{I_0},$$

and,

Z_0 : length of anode,

$t_0 = \sqrt{(L_0 C_0)}$: discharge characteristic time,

$I_0 = V_0\sqrt{\frac{C_0}{L_0}}$: "short circuit" current.

Using a scaling parameters as:

$$\alpha = \frac{t_0}{t_a} \quad \text{: time parameter,} \tag{3.6}$$

where,

$t_0 = \sqrt{(L_0 C_0)}$: discharge characteristic time,

$t_a = \sqrt{\frac{4\pi^2(b^2 - a^2)}{\mu_0 \ln(\frac{b}{a})}(\frac{\Gamma - 1}{\Gamma})\frac{\rho_1 z_0^2}{I_0^2}}$: dynamic characteristic time,

$\frac{z_0}{t_a}$: characteristic speed,

$\beta = \frac{L_a}{L_0}$: inductance ratio, (3.7)

where,

$$L_a = \frac{\mu_0}{2\pi}\frac{\Gamma - 1}{\Gamma}\ln(\frac{b}{a})z_0 . \quad (3.8)$$

The density of an ambient gas can be calculated by,

$$P = nkT$$
$$= \rho_1 \frac{R_o}{M} T , \quad (3.9)$$

where,

n = mole,

k = Boltzman constant (1.3806x 10^{-23} $\frac{J}{K}$),

T = temperature (K),

ρ_1 = density of ambient gas,

R_o = Gas constant (8.3144 $\frac{J}{mole \cdot K}$).

For the first simulation model, we estimated β, α and set dt with a suitable time interval value. From a current measurement of the plasma focus the time period t_o can be measured. The time period of current signal is 12.28 μs.

From $t_o = \frac{T}{2\pi}$ and $t_o = \sqrt{(L_o C_o)}$,

we can calculate,

$$L_o = \frac{t_o^2}{C_o} = \frac{T^2}{4\pi^2 C_o}$$

$$= \frac{\left(12.28 \cdot 10^{-6}\right)^2}{4\pi^2 \cdot 30 \cdot 10^{-6}} \quad = 127.33 \text{ nH.}$$

Then using Equation 3.8 and assuming $\frac{\Gamma-1}{\Gamma}\approx 1$, a = 0.95 cm, b=3.2 cm, z_o=16 cm

$$L_a = \frac{1.256637\cdot 10^{-6}}{2\cdot\pi}\ln\left(\frac{3.2}{0.95}\right)\cdot 16\cdot 10^{-2}$$

$$= 2\cdot 10^{-7}\cdot 1.21\cdot 16\cdot 10^{-2}$$

$$= 38.72 \text{ nH.}$$

Therefore, from Equation 3.7

$$\beta = \frac{L_a}{L_o} = \frac{38.72\text{nH}}{127.33\text{nH}} = 0.30409.$$

By using $\beta = 0.30409$ for the simulation, and allowing the current signal goes to zero at the end of anode. α can be estimated to be equal to 0.452174. Figure 3.11 shows the results from the simulation.

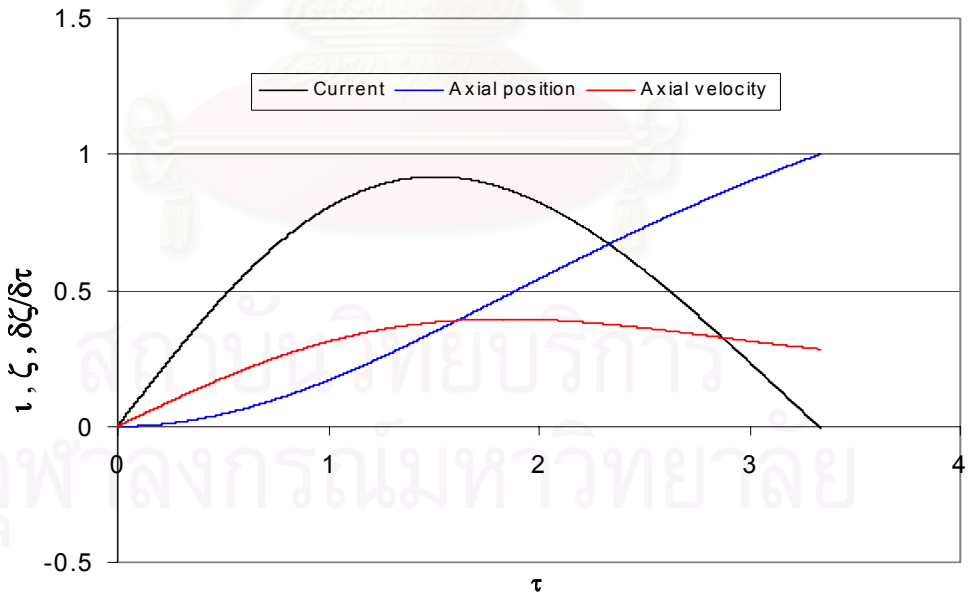

Figure 3.11: A graph showing current, axial position and axial velocity results of axial phase with respect to time from the numerical computation.

P(torr)	ρ_1	Vo(kV)	Io(kA)	Zo(cm)
3.75	0.002770739	12.0	176.9303	9.7319
0		12.5	184.3024	10.1374
		13.0	191.6745	10.54289
		13.5	199.0466	10.94839
		14.0	206.4187	11.35388
3	0.002216591	12.0	176.9303	10.88059
		12.5	184.3024	11.33395
		13.0	191.6745	11.78731
		13.5	199.0466	12.24067
		14.0	206.4187	12.69403
2.25	0.001662443	12.0	176.9303	12.56383
		12.5	184.3024	13.08732
		13.0	191.6745	13.61081
		13.5	199.0466	14.13431
		14.0	206.4187	14.6578
1.5	0.001108296	12.0	176.9303	15.38748
		12.5	184.3024	16.02863
		13.0	191.6745	16.66978
		13.5	199.0466	17.31092
		14.0	206.4187	17.95207
0.75	0.000554148	12.0	176.9303	21.76119
		12.5	184.3024	22.66791
		13.0	191.6745	23.57462
		13.5	199.0466	24.48134
		14.0	206.4187	25.38805

Table 3.5: A table showing the results from the numerical simulation.

Table 3.5 shows the condition of the currents and voltages used for experimental conditions in order to allow the current sheath to arrive at the end of the anode at the same time as the current goes to zero.

In the simulation $\frac{\Gamma - 1}{\Gamma} = 1$ is used. By using the time when the focusing occur, the $\frac{\Gamma - 1}{\Gamma} = 0.09$ is obtained. This values is used for the calculation of α and β which are found to be 0.4445 and 0.0274 respectively. It was found that the pressure when the current signal goes to zero at the same time when the plasma sheath reaches the end of anode is 5.5 mbar. The simulation is shown in Figure 3.12.

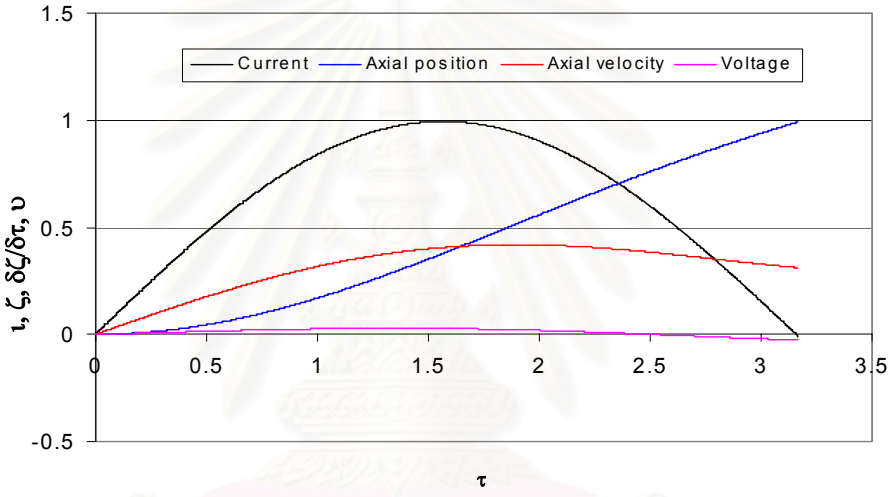

Figure 3.12: A graph showing current, axial position and axial velocity results of axial phase with respect to time from the numerical computation where α is 0.4445 and β is 0.0274 after the fitting from experiment result.

3.3 Measurement of Instantaneous Velocity of Plasma Sheath

As described in Section 2.4.3, an instantaneous velocity of the plasma or current can be measured by using double magnetic coils or the magnetic probe. The change of this quantity with time or position will gives us an insight to the acceleration of the plasma sheath which is the result of the $\vec{J} \times \vec{B}$ force.

In this measurement, the magnetic probe was placed through the top plate of the plasma focus between the anode and cathodes as shown in Figure 3.13. The depth of the coil was measured each time. This determines the position of the instantaneous velocity measured. The magnetic coil was inserted in an insulating glass tube. The magnetic probe was placed carefully in order to ensure the correct orientation of the coil. The plane of the magnetic coil must be perpendicular to the magnetic field for maximum signal.

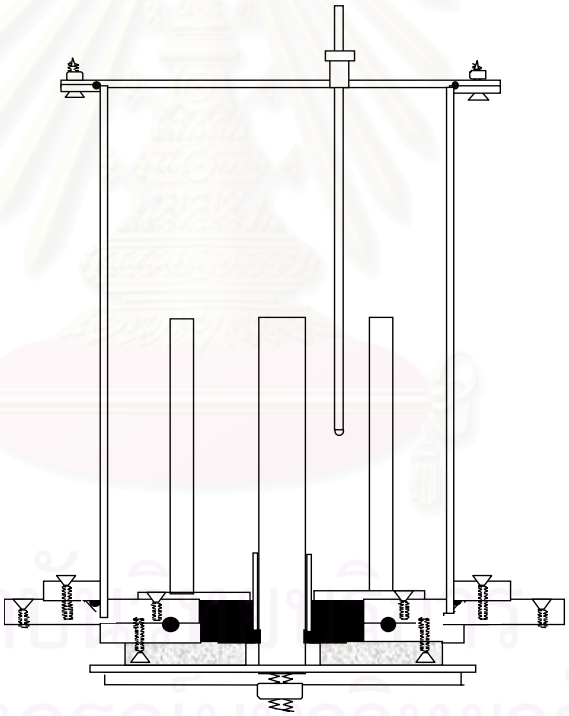

Figure 3.13: A diagram showing the position of a magnetic probe, which is placed in between the anode and cathode of the plasma focus.

Gas	Nitrogen		Argon	
Velocity / Pressure (mbar)	1-2 (cm/μs)	2-3 (cm/μs)	1-2 (cm/μs)	2-3 (cm/μs)
0.5	6.855	6.084	6.380	4.079
1.0	5.905	5.220	5.405	3.868
1.5	5.287	4.034	4.174	3.010
2	4.032	3.444	3.959	2.833
2.5	3.096	2.983	3.170	2.466
3	1.789	1.787	2.391	1.645

Table 3.6: A table showing velocities of Nitrogen and Argon plasma for the short hollow anode.1-2 is the velocity of 1st probe to 2nd probe and 2-3 is the velocity of 2nd probe to 3rd probe.

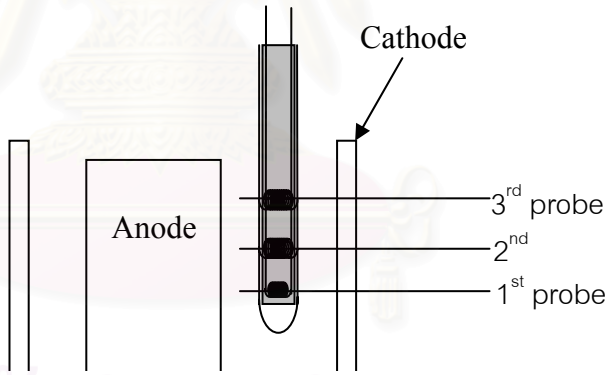

Figure 3.14: A diagram showing positions of magnetic probe in the plasma focus tube.

The 1st probe detects the magnetic field from the plasma sheath before 2nd probe and 3 rd probe. By the time difference and the different in position, the velocity can be determined.

The distance between 1st probe and 2nd probe is 0.92 cm. The distance between 2nd probe and 3rd probe is 0.72 cm. The positions of the three probes are

shown in Figure 3.14. Table 3.6 shows the velocities of the plasma sheath by using three magnetic probes. The signals of the three probes are shown in Figure 3.15.

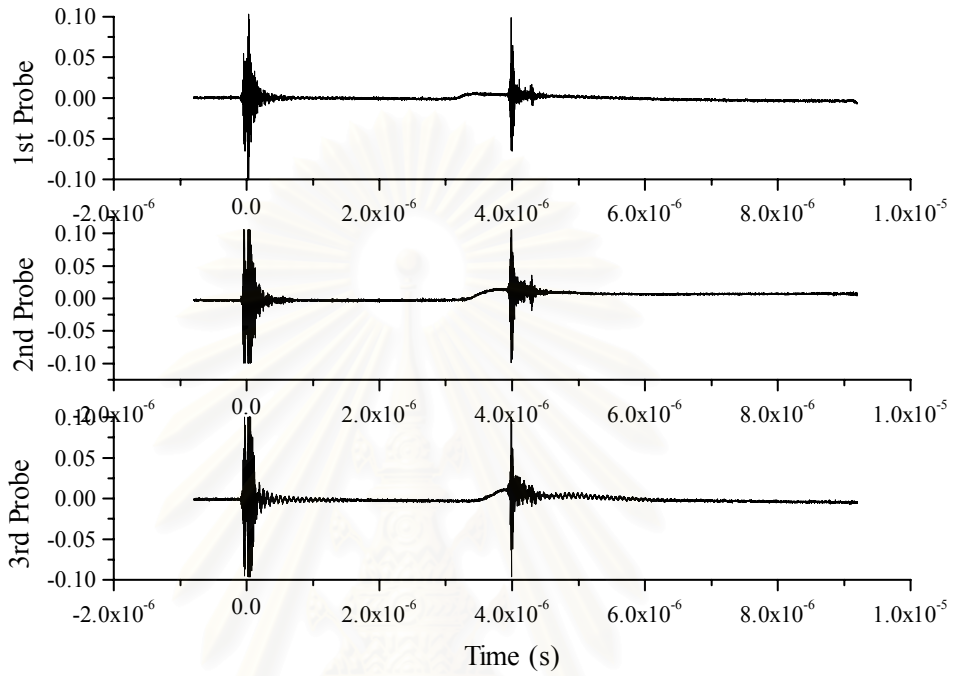

Figure 3.15: Graphs showing signals from magnetic probe placed at three different positions in the plasma focus for Nitrogen plasma at a pressure of 1.5 mbar.

The relationship between ln(v) is linear with pressure. This is shown in Figure 3.16 and Figure 3.17.

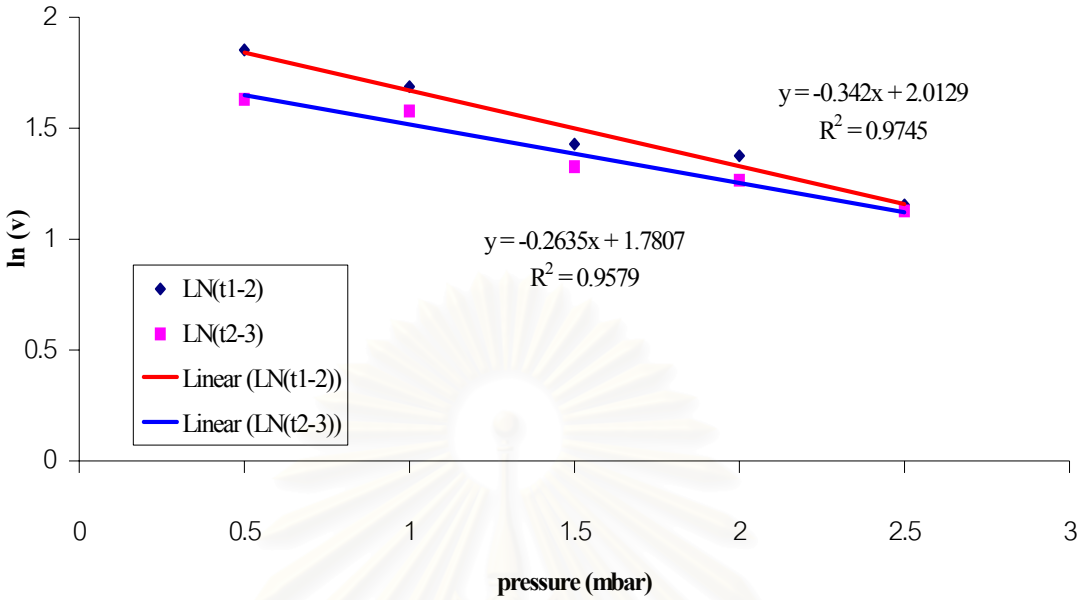

Figure 3.16: A plot showing a relationship between pressure and in stantaneous velocity of Nitrogen plasma sheath.

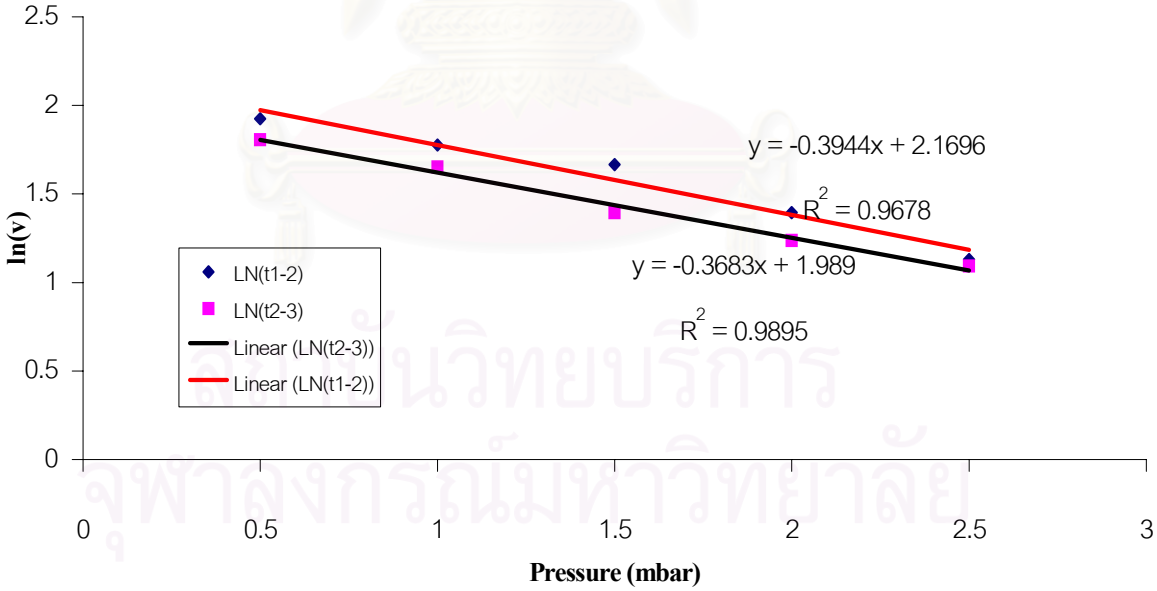

Figure 3.17: A plot showing a relationship between pressure and instantaneous velocity of Argon plasma sheath.

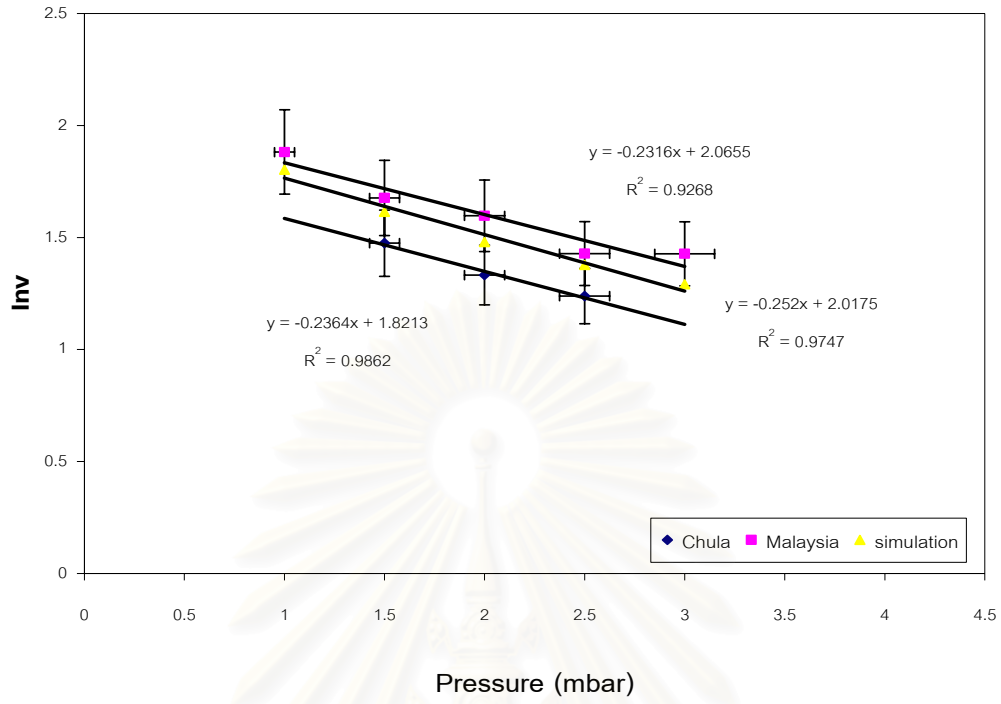

Figure 3.18: Graphs showing a comparison of results from different plasma focus devices operated with argon gas [27].

Figure 3.18 shows results from the plasma focus used in this experiment in comparison with a similar plasma focus device in University of Malaya. Both results are in good agreement with the axial phase simulation.

3.4 Measurement of Plasma Jet Velocity

The plasma jet experiment was carried in the Plasma Laboratory, University of Malaya, Malaysia. The system used in this experiment is a similar system to the 3.3 kJ UNU/ICTP plasma focus device. The anode and the cathodes are of the same length at 16 cm long. Nitrogen gas was used in this experiment. The experiment is separated into two parts. In the first part, a single probe as described in Section 2.4.4 was used to measure ions or plasma. In the second part, multiple probes

measurement was carried out, where the chamber was extended with an additional 3 ports chamber. A two stage rotary pump was used in order to achieve the desire vacuum in this larger chamber. The charging voltage used through out the experiment was 12.5kV.

In measuring the plasma jet, both focusing and non-focusing cases were studied. These can be achieved by varying the operating pressure. The pressures used for the experiment were 1 mbar and 2 mbar for the focusing case and 3 mbar, 4 mbar, 5 mbar, 6 mbar, 7 mbar, 8 mbar, and 9 mbar for the non focusing case. Before each experiment can be carried out, it is important to find a correct operating bias voltage of the electric probe. A good signal to noise must be achieved in order to identify the real plasma jet or ion signal.

3.4.1 Finding Correct Bias Voltage for Electric Probe

This series of experiments were carried out with an aim to find out a suitable biasing voltage for the electric probe in order to get a good signal to noise ratio. A single electric probe was used to measure the ions from the plasma jet. The probe was connected to a bias circuit as shown in Figure A5 in Appendix A. It was placed at 8.5 cm from the end of anode through the top plate of the plasma focus (Figure 3.19). Nitrogen gas was used in this test. The test was carried out under two pressure regimes, 1 mbar and 3 mbar for focusing and non-focusing purpose.

Bias voltage of -10V, -20V, -50V, -100V, -150V, -200V, -250V, -300V had been tested. From the test, a bias voltage at -200 V gave an optimum signal.

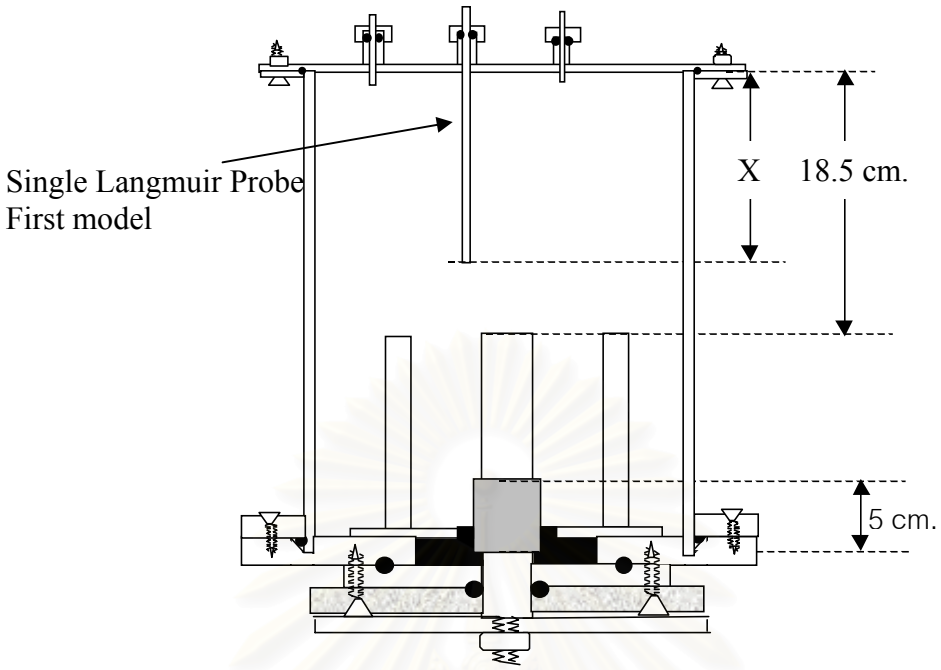

Figure 3.19: A diagram showing the position of an electric probe at distance X from the tip of the anode.

3.4.2 Determination of Plasma Jet Velocity

Once the probe's bias voltage was determined, the probe was then used in an experiment to measure the velocity of the plasma jet. For a non-focusing experiment, a pressure of 3 mbar was used. The probe was placed at different positions for spatial measurement. Figure 3.19 shows the arrangement of the probes. However, with this set up the results obtained were not suitable for velocity determination. The result is shown in Figure 3.20.

It is interesting to see that, with this method the calculated velocity of the plasma jet behave as expected. As the traveling distance increases the average velocity of the plasma jet decreases. An obvious cause for this is the collision of the traveling atomic particle with the ambient particles in the chamber. The relationship of the average velocity and the travelled distance is shown in Figure 3.20.

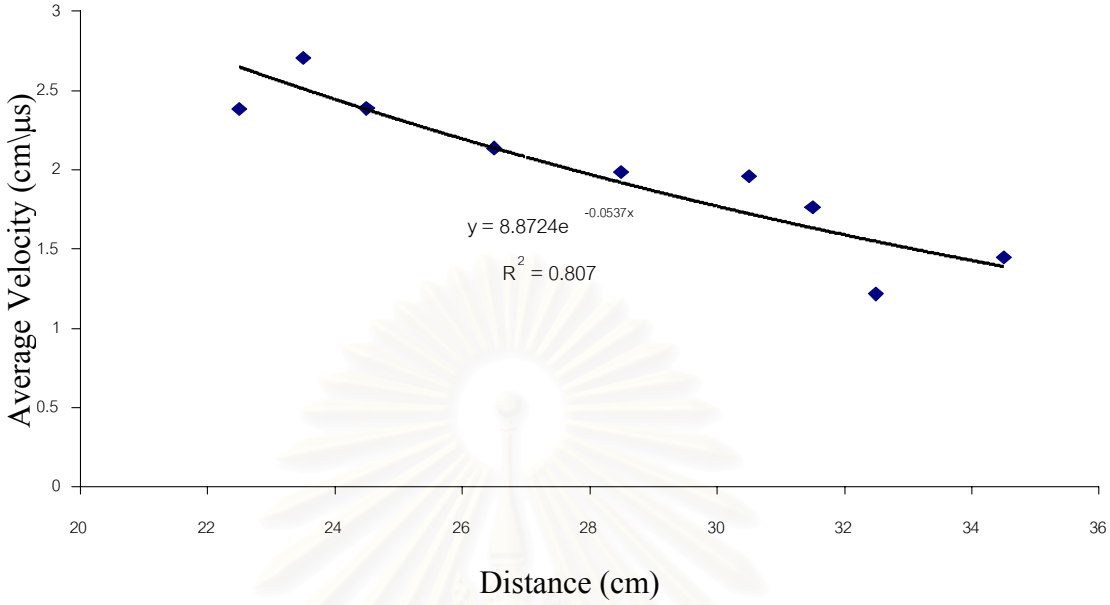

Figure 3.20: A graph showing a relationship between average velocity of the plasma jet and the distance of the probe away from the tip of the anode.

In the next step, the simulation explained in Section 3.2 was used to estimate the time reference when the plasma jet is expelled from the tip of the anode by varying the pressure. The reference point is set such that when the current reaches zero the plasma sheath also reaches the end of the anode.

In the section 3.2 the condition for Nitrogen (A=7 and Z=28) plasma is at a pressure of 3.75 torr for a capcitance of 30 μF and the anode length of 16 cm operating with 12.5 kV charging voltage.

For a better measurement of the plasma jet velocity, two single probes of the second model (Section 2.4.4) were used at the same time. The arrangement is shown in Figure 3.21(b). The detection area of these probes is 2 cm long.

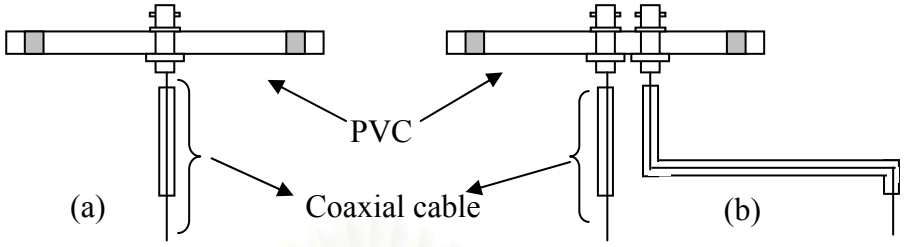

Figure 3.21: Diagrams showing different electric probe set up (a) with one electric probe and (b) with two electric probes.

Distance of the probes was adjusted to measure signal at different positions. The first probe was placed at 11 cm away from the end of the anode. Another probe was placed at 27 cm. The pressure used was the same as the simulation result. The experimental set up is shown in Figure 3.22. The charging voltage used was 12.5 kV.

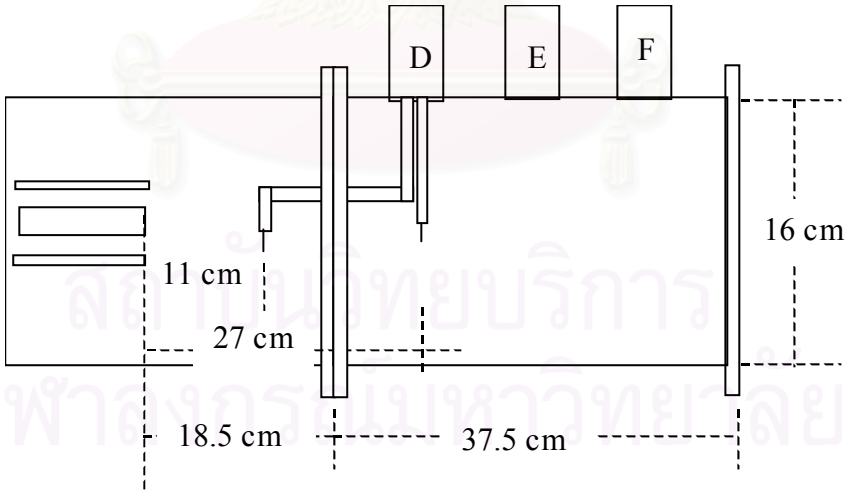

Figure 3.22: A diagram showing the placement of two electric probes. One electric probe is 11 cm away the other electric probe is 27 cm away from the tip of the anode.

It is interesting to note that, the probe break down when a bias of –150 V was used. Therefore a bias of -130 V and -120 V were used instead. Example of the signals is shown in Figure 3.23.

The result is a negative pulse changing with time. We can see clearly that the signal rises at 1.0×10^{-5} s and rises again at 2.0×10^{-5} s. This second rise in signal may be contributed by the plasma jet. The experiment was repeated, except that this time the signal is detected without bias. The result is shown in Figure 3.24.

This time we obtained a positive pulse. It is suspected that the region labeled may be the peak caused by the detected plasma jet.

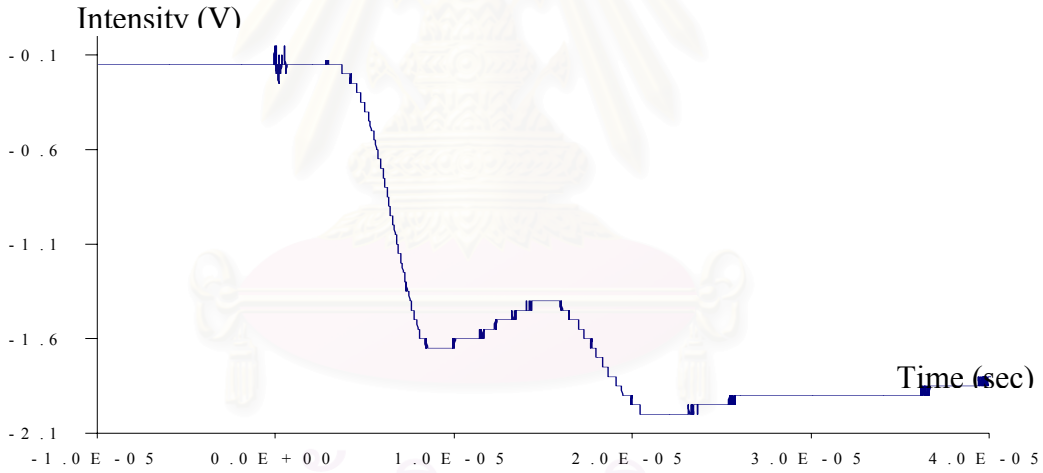

Figure 3.23: A graph showing the signal from the first electric probe when operated with -130 V bias voltage.

Since the signal is large, with the above configuration, as shown in Figure 3.23 and Figure 3.24, and the time that the peak started is close to the focusing time, it is necessary to move the probe out to a larger distance in order to be able to distinguish the plasma jet clearly. The set up is shown in Figure 3.25.

From many results, the best signals were obtained when the electric probes were not biased. With this set up, we used the electric probes to measure the

presence and the speed of the plasma jet. A similar technique of time of flight as the experiment to determine the speed of the plasma sheath was used to determined the speed of the plasma jet, both in focusing and non-focusing mode.

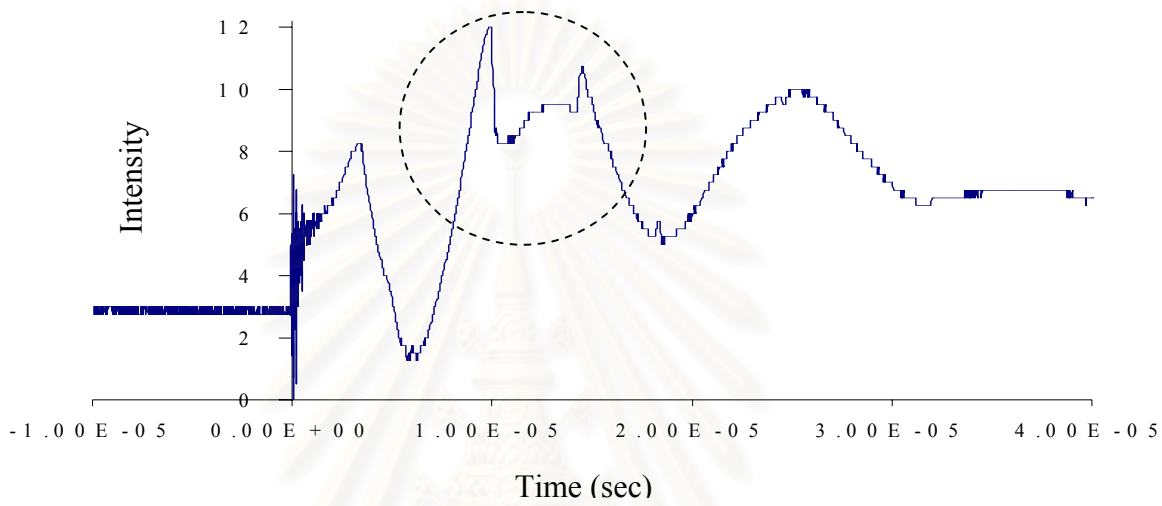

Figure 3.24: A graph showing the signal from the first electric probe when operated without bias voltage.

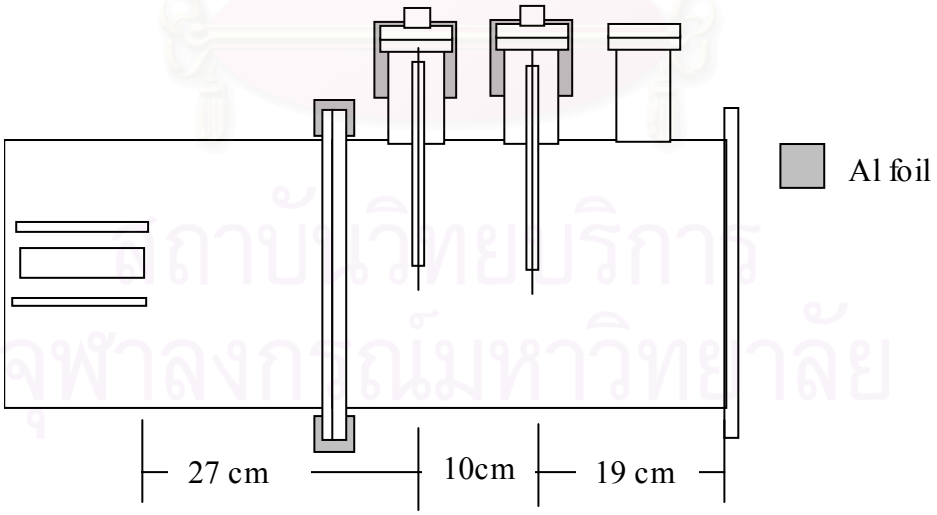

Figure 3.25: A diagram showing the placement of two electric probes. One electric probe is 27 cm away the other electric probe is 37 cm away from the tip of the anode.

3.4.3 The Velocity of Focused Plasma Jet

The velocities of the plasma jet are estimated with time of flight (TOF) method from the two electric probes. The first probe and second probe was placed at 27 cm and 37 cm from the end of the anode respectively. Both electric probes were connected to a x1 attenuator which matched the coaxial cable. A typical measured signal is shown in Figure 3.26.

In general, two groups of signals were observed. The first group happened immediately after the focus and the second group happened at a later time. This means that the signal from the second group may be contributed by slower moving particles. The experiments were repeated for seven different pressures from 1 mbar to 7 mbar.

At 1 mbar and 2 mbar, usually both groups of signal appear, but in some case only the second group appear. After analyzing the data, it is probable that the group one only appears when the plasma focused. Therefore it is lead to believe that the focusing process of the plasma causes ejection of energetically charged particles. Thus the plasma focus, when focusing, can produce ion beam. This confirms the finding from many literatures mentioned in previous chapter. The first peak observed in the group one signals by probe 1 and probe 2 are labeled peak 1a and 1b in Figure 3.26. A comparative result of the average velocity of the ion and the plasma jet is shown in Table 3.7. We can see that the plasma jet has a speed of 100 times slower than the ions.

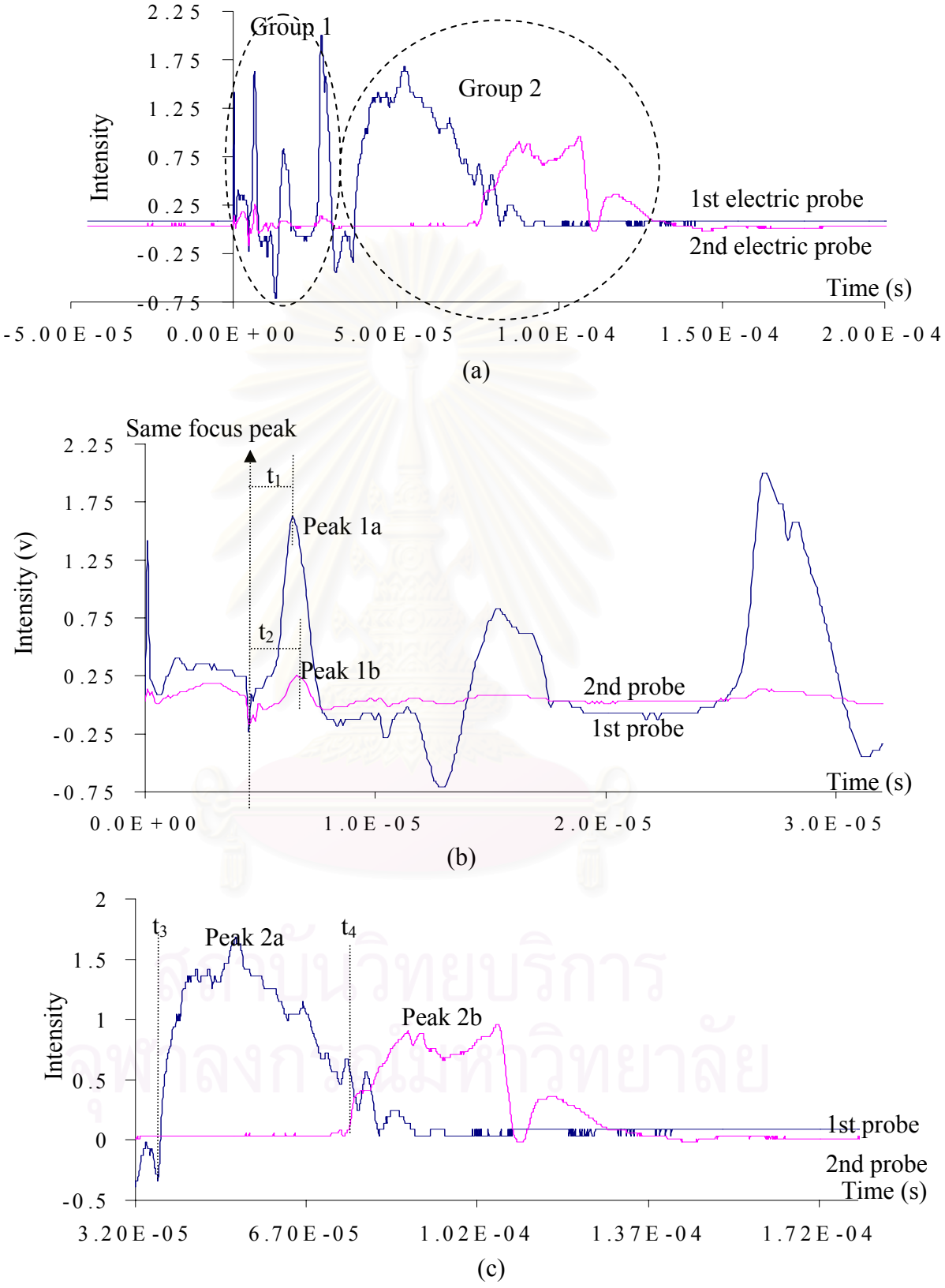

Figure 3.26: Graphs showing the signal obtained from the first and second electric probe where (a) is the overall signal, (b) is group an enlargement of the first group of signals and (c) is the enlargement of the second group of signals.

Pressure(mbar)	Average velocity of group 1 (cm/μs)	Average velocity of group 2 (cm/μs)
1	46.74	0.3578
2	36.70	0.2576

Table 3.7: A table showing average velocities of group 1 (signals from peak 1a and peak 1b) and group 2 (signals from peak 2a and peak 2b)

3.4.4 The Velocity of Non-Focused Plasma Jet

For the measurement of the plasma jet in a non-focused mode, a similar experimental set up as previous section was used. This time the operating pressure was set at a higher pressure of 3 mbar, 4 mbar, 5 mbar, 6 mbar, and 7 mbar, where the plasma will not focused. The velocities of the plasma jet are estimated with the time of flight technique. A typical signal is shown in Figure 3.27.

In this case, groups of plasma jet can be seen clearly in all the pressures. The velocity of the plasma jet at different pressures are shown in Figure 3.28. We can see that the velocity of the plasma jet decreases as the pressure increases. This is expected.

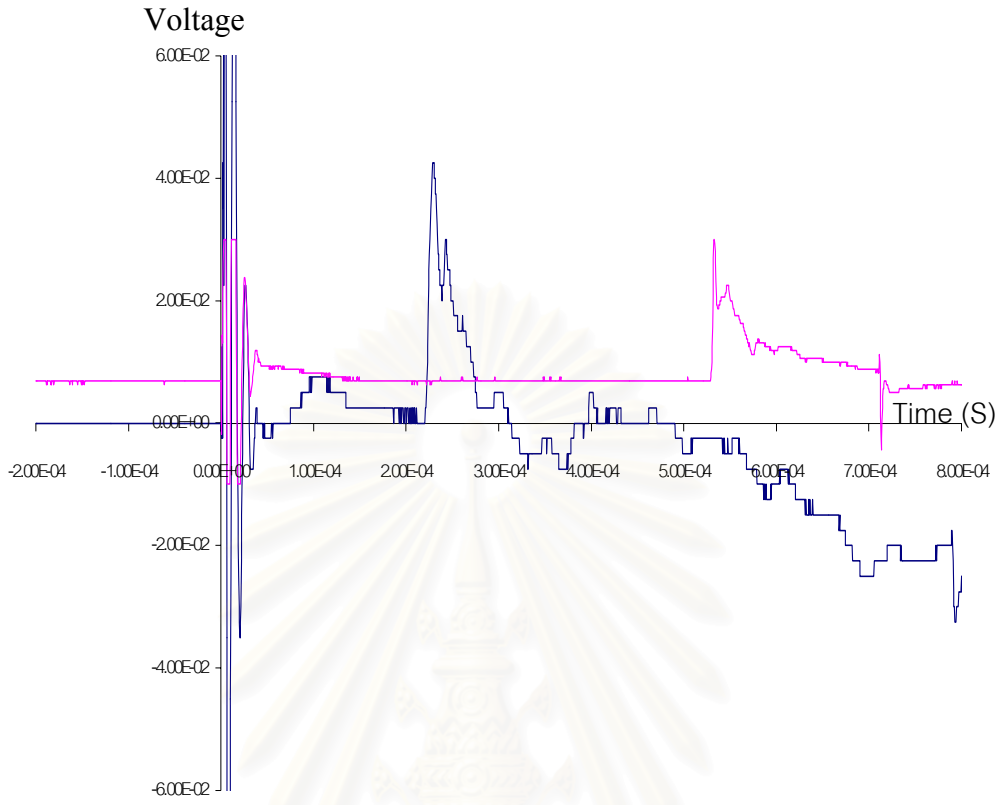

Figure 3.27: A graph showing a signal of the plasma jet when the plasma focus is operated with pressure of 7 mbar.

In order to study spatial effect on the velocity, the number of probe was increased. Two initial probes were at the same distance as previous. Another two probes were added to the port E an F. The signals of all the probes are shown in Figure 3.29. It can be seen that the average velocity of the plasma jet decreases as it gets further away from the anode. The average velocity seems to decrease exponentially with pressure and decreases more than 300% within 10 cm.

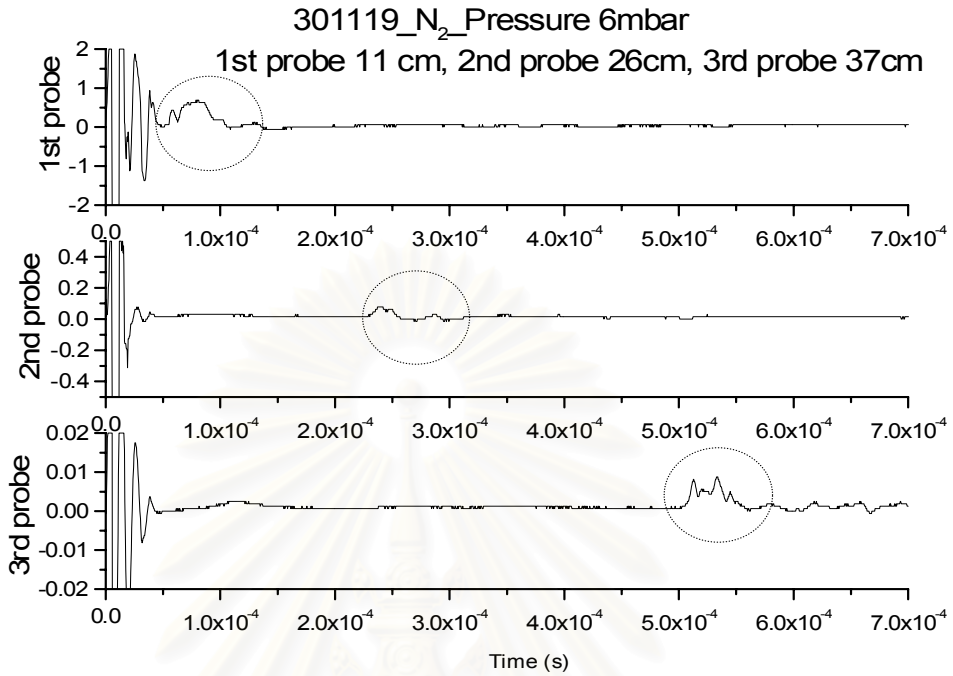

Figure 3.28: Graphs showing signal of three electric probes where the first probe is placed at 11 cm and the second probe is at 26 cm and the third probe at 37 cm away from the tip of the anode

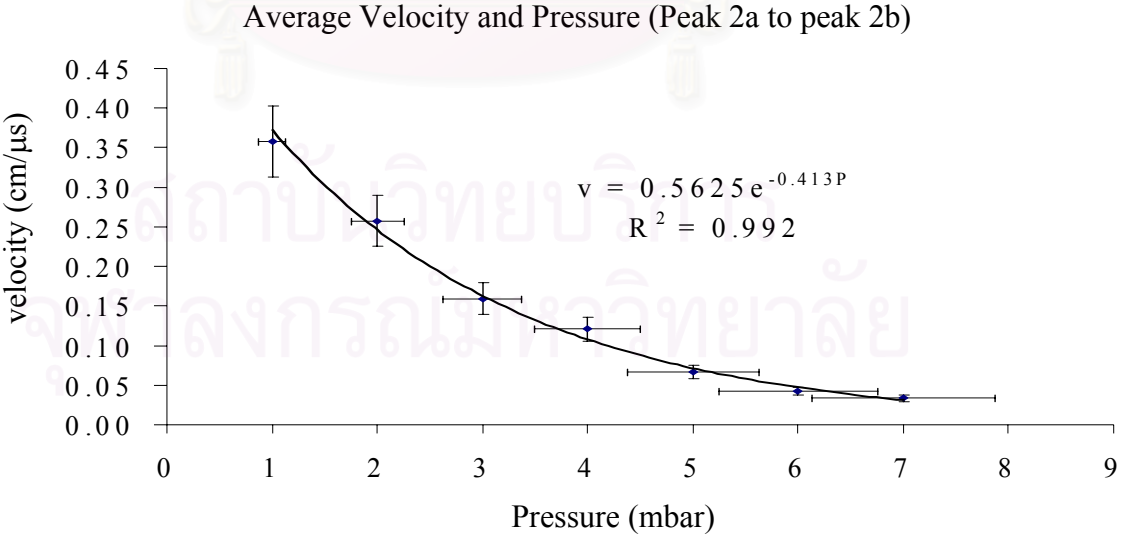

Figure 3.29: A graph showing a relationship between the velocity of the plasma jet and changes in pressure.

CHAPTER 4

MATERIAL SURFACE MODIFICATION

As described in Chapter 1, many attempts have been made in using plasma focus device for material surface modification purpose. In this chapter, various experiments on material surface modification are explored. The experimental conditions used are similar to the condition described in Chapter 3 for various cases including, the focused, non-focused mode and the plasma jet. In general, for each firing of the plasma focus the voltage signal is recorded. The pressure for the operating gas is between 0.5 mbar to 2.5-mbar for Nitrogen gas and 0.5 mbar to 2.0 mbar for Argon gas. For the non-focusing mode, the pressure used is more than 3 mbar.

Different types of materials were investigated under this modification process which can be classified as insulating substrate and conducting substrate such as thin aluminum plate, titanium plate and steel plate. The changes in the surface properties which are of interest are the change in hardness, coating of new material and damage caused by the plasma.

4.1 Surface Coating on Insulating Substrate

In the Plasma Research Group, Physics Department, Faculty of Science, Chulalongkorn University, there are many projects related to this work which have been carried out. During the period of my research I had an opportunity to take part in some of these projects.

One of the works done in 2000 [12] is using a plasma focus to coat metal on insulating substrate, in that case copper and glass respectively. In this experiment Argon gas was used. The operating pressure was set to 0.5 mbar as this pressure would provide the strongest focus as shown in Section 3.1. The sample was glued on the top plate at 12.5 cm in front of the anode as shown in Figure 4.1. At least twenty shots were fired.

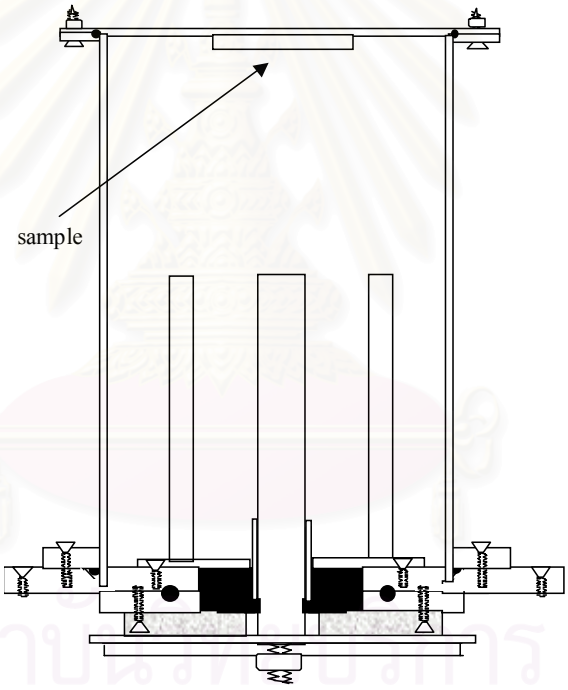

Figure 4.1: A diagram showing the position of sample investigated

Figure 4.2: Pictures showing copper coating on glass insulator when placed at 12.5 cm away from the tip of the anode and firing with Argon at a pressure of 0.5 mbar [12].

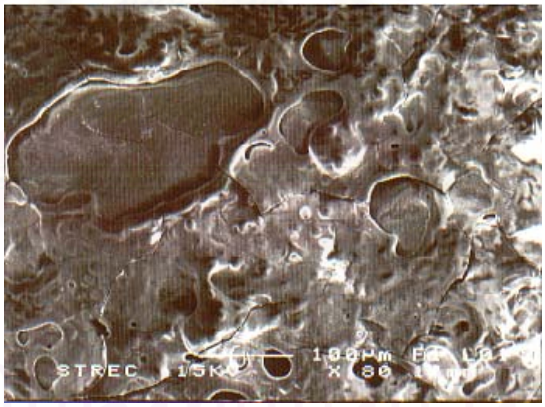

Figure 4.3: A picture of the surface of the glass substrate coated by copper taken by SEM [12].

The copper coating on the glass surface is shown in Figure 4.2. A sign of damage from the focusing process is very apparent. Figure 4.3 shows a magnification of the coating surface from a Scanning Electron Microscope (SEM).

The surface is bombarded by ions from the focus as well as there may be heating effect due to the shock wave generated by the plasma focus.

4.2 Surface Damage by Focusing Effect

To study more into the damaged, a thick Aluminum plate was placed at 2 cm in font of the anode. The operating pressure was 1 mbar. Ten shots were fired. The treated sample is shown in Figure 4.4.

Figure 4.4: A picture showing the damage caused by the bombardment of plasma on the surface of the Aluminum plate which was placed at 2 cm away from the tip of the anode in Argon gas.

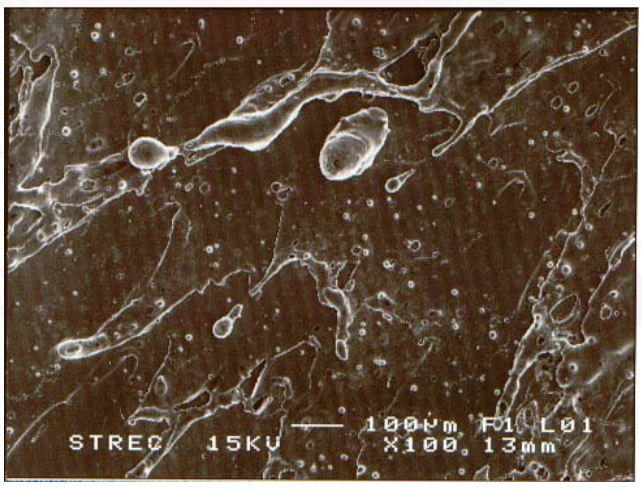

Figure 4.5: A picture showing the surface of the aluminum sheet enlarged at x1000 by SEM.

Figure 4.5 shows a x100 magnification by SEM of the thick aluminum sheet. We can see that the damage trail has a resemblance to liquid droplet. This is a good evidence of heating and 'flushing' effect causes by the focus on the metal surface. There is little evidence of ions bombarding. It is suspected that, at this close range to the anode the current sheath flushes through the surface as well as heating the plate.

Further experiment to support the heating effect of the plasma was carried out. A larger piece of aluminum plate with a diameter of 7.5 cm was used. The plate was placed at 7.5 cm away from the anode. An operating pressure was set at 0.5 mbar allowing for maximum focusing. Fifty shots were fired under this condition.

From Figure 4.6, the damages can be divided into three zones. First zone is the most heavily damaged where the surface of the plate is roughest. It is suspected that the ions bombardment may be the cause. In the second zone, there are sign of color change which resemble that of metal being under intense heated. This region may be caused by the heat of the hot plasma or hot gas. Further out to the third zone there is no observable effect. This shows anisotropy of the moving plasma. The plasma or ions produced has a good directionality.

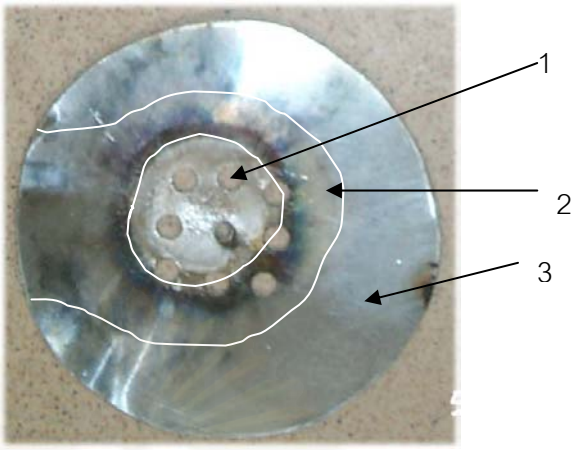

Figure 4.6: A picture showing the three-zone effect caused by the focusing of the plasma on the surface of Aluminum. In the first zone, the surface is bombarded by ions. In the second zone, the plasma heats the surface. There is no effect in the third zone.

4.3 Study of Titanium Nitride Deposition

In my research, a special attention has been paid to the study of Titanium Nitride (TiN). The plasma focus was configured such that the Titanium piece is glued to the top plate allowing the direct bombardment of plasma and ions from the focus.

In this experiment, an attempt has been made to modify the surface of Titanium directly with Nitrogen plasma from the plasma focus. The set up of the experiment is shown in Figure 4.8. The sample is separated by a masking Mylar into two areas. Each area represents different operating conditions as shown in Table 4.1. The size of the Titanium plate is 1cm x 1 cm. For area 1, the sample was placed at 13.5 cm away from the anode. Ten shots were fired. A record of firing condition is shown in Table 4.1.

Shot-no	Signal	Pressure	Charging voltage
1	No-focusing	1.5 mbar	13.0 kV
2	No-focusing	1.5 mbar	13.0 kV
3	No-focusing	2.0 mbar	13.0 kV
4	Focusing	0.5 mbar	13.0 kV
5	Focusing	0.5 mbar	13.0 kV
6	Focusing	0.5 mbar	13.0 kV
7	Focusing	1.0 mbar	13.0 kV
8	Focusing	0.5 mbar	13.0 kV
9	Focusing	0.5 mbar	13.0 kV
10	Focusing	0.5 mbar	13.0 kV
11	Focusing	0.5 mbar	13.0 kV
12	Focusing	0.5 mbar	13.0 kV
13	focusing	0.5 mbar	13.0 kV

Table 4.1: A table showing the experimental conditions for the Ti-plate.

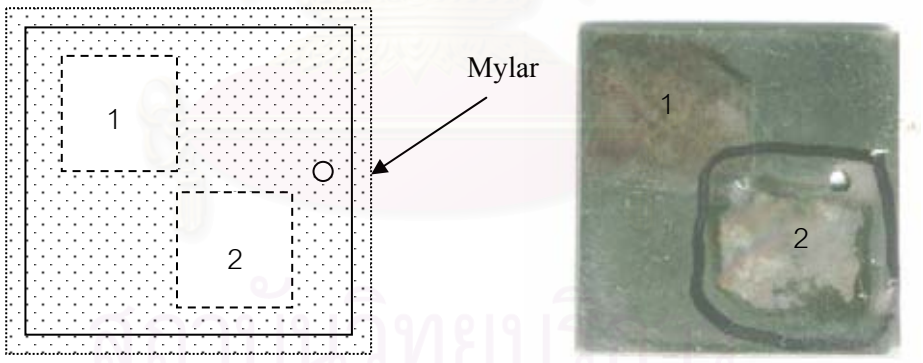

Figure 4.7: A diagram and a picture showing the two zones allocated on a Ti-plate. Zone one shows an evidence of copper coating where zone two shows damage effect by ion.

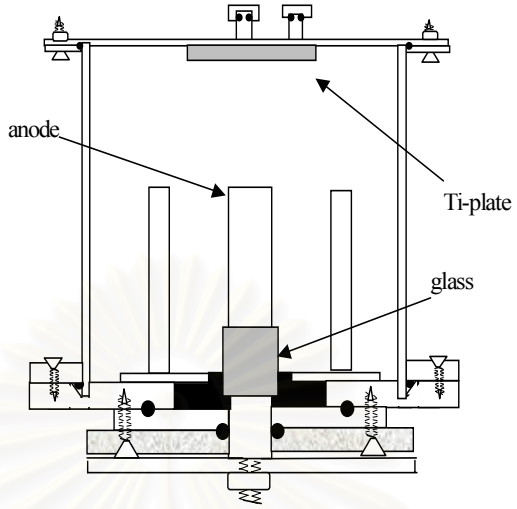

Figure 4.8: A diagram showing the position of the Ti-plate.

It can be seen that in this area there are some traces of copper. The copper is coated on the surface as shown in Figure 4.7. Since the anode is made from a copper rod, it is speculated that the copper may have only come from the anode. This speculation is backed by the damaged observed at the tip of the anode where there is a sign of corrosion.

For the second area, the Titanium Plate was placed at 13 cm away from the anode. Fifty shots were fired under an operating pressure of 0.5 mbar for an optimum focusing shot. The charging voltage was set at 13 kV for all shots. There was focusing in every shot. The surface of the Ti plate was scanned by Scanning Electron Microscope and Energy Dispersive X-ray Diffraction (EDX) for elemental trace identification. The results are shown in Figure 4.9 and Figure 4.10 respectively.

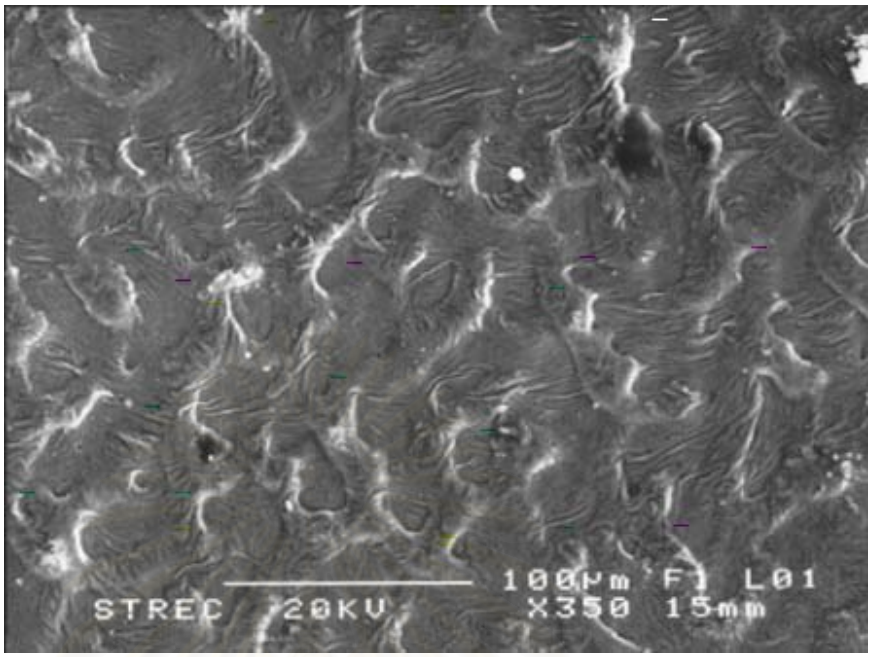

Figure 4.9: An enlarged (x350) picture of the surface of the Titanium plate in zone two taken by SEM.

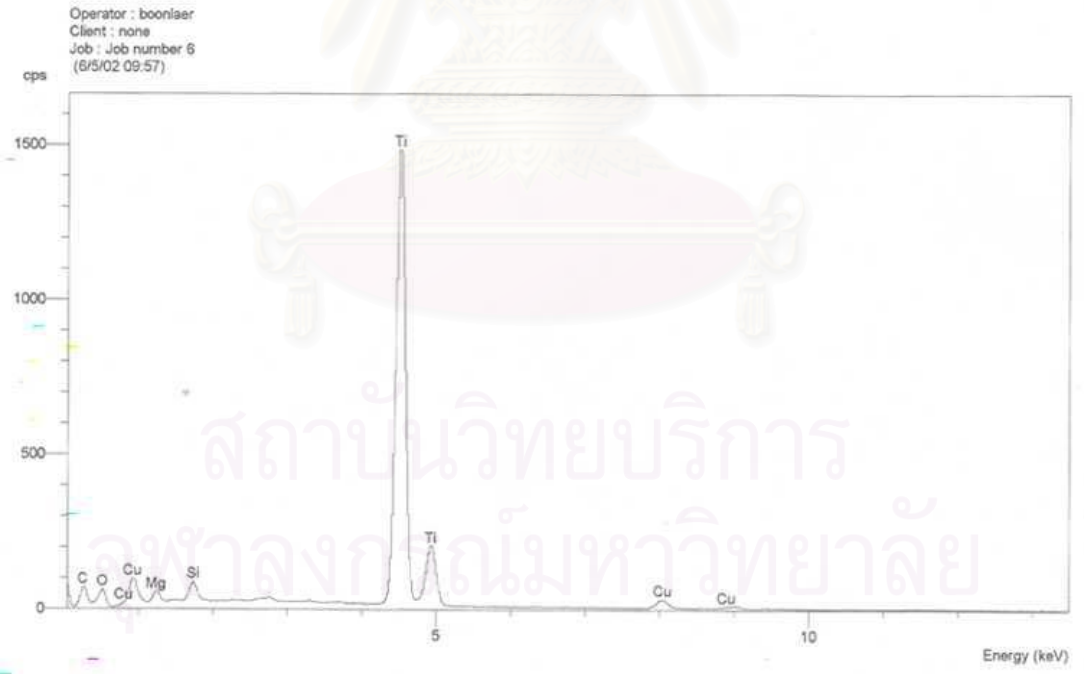

Figure 4.10: A graph showing the result from EDX analysis of the surface of the Titanium plate in zone two giving its composition.

Since Titanium is a much harder metal than aluminum, we can see that the damage caused by the plasma focus is less, but some evidence of change can still be observed. This change is possibly caused by the bombardment of the plasma or energetic ions. In the same time, EDX result shows and confirms a clear trace of copper on the surface of the Titanium plate.

In a similar experiment, another Titanium plate was placed at 17 cm in front of the anode. In this experiment the firing of the plasma focus was separated into two stages. The first stage is where 20 shots were fired with the first ten shots at 2 mbar operating pressure and the subsequent ten shots were at 1.5 mbar. After the first ten shots, the sample was taken out for observation. There was no observable change on the surface of the Titanium plate. After the twentieth shots, the sample was observed again. A clear yellow color can be observed on the surface of the plate. This yellow coating may be Titanium Nitride. This yellow color can be seen on the sample in Figure 4.11. A SEM picture of this is shown in Figure 4.12.

After firing the focus in the second stage using 1 mbar operating pressure for twenty shots, a sign of heavily damaged surface appeared. This is observable by eye. This damaged is shown in Figure 4.11. Since all the shots in this stage produced strong focusing, the particle beam produced by the focus may cause this damage to the surface. It is unlikely that Titanium Nitride can be coated in the focusing mode as the damaged caused by the focus is quite severe in every shots.

Figure 4.11: A picture showing the surface of the Ti-plate bombarded by ions.

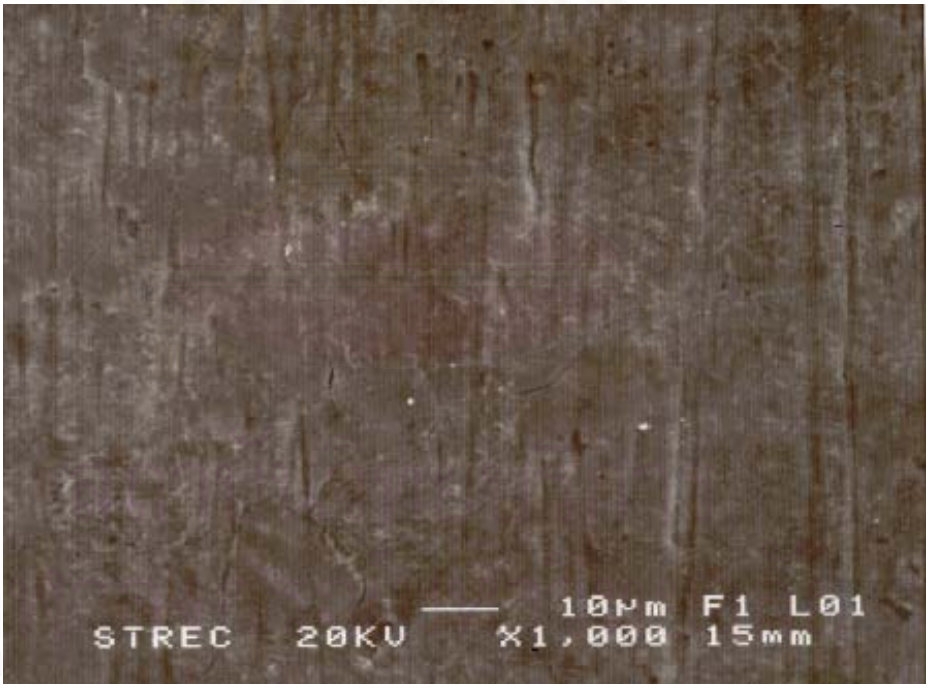

Figure 4.12: A picture taken from SEM of the gold area of the Ti-plate at which was placed 17 cm away from the tip of the anode when firing.

Therefore, it is obvious that for a successful coating we must use the plasma focus in a non-focusing mode or alternatively move the sample to a further distance. In the next experiment, the Titanium plate was placed at 31 cm away from the end of the anode. The operating pressure was set to be at 0.5 mbar and the charging voltage of 13 kV. Ten shot were fired and all shot focused. A desired color change was observed. This is shown in Figure 4.13.

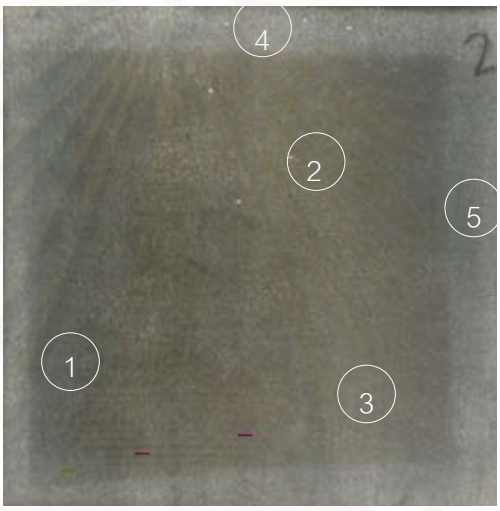

Figure 4.13: A picture showing the position for the hardness test on the Ti-plate after treated with the plasma focus.

Figure 4.14 shows an image of the sample from a microscope with X10/0.22 magnifying power. Unfortunately the result from EDX did not show the trace of nitride. Therefore a hardness test was performed in order to support the change of the surface property.

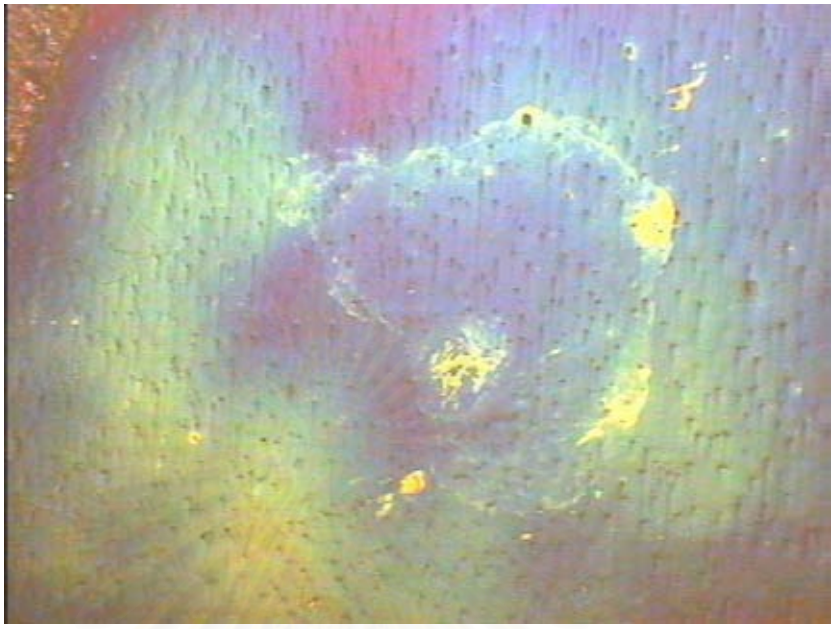

Figure 4.14: A picture of the surface of the Ti plate taken from a microscope.

A hardness was made using WILSON 500 (Model B534-T). The random positions of the test point for pressing on the Titanium plate are shown in Figure 4.13. The results of this hardness test are shown in Table 4.2.

Position	Hardness (HV3)
1	151
2	145
3	145
4	141
5	142

Table 4.2: A table showing the result of the hardness test (by WILSON 500 Model B534-T) on the Ti-plate after plasma focus treatment.

We can see from the table that there are slight changes in hardness when comparing the hardness measured between the treated surfaces (1,2 and 3) and original surfaces (4 and 5). These results are by no means conclusive. Further tests are

required to confirm this result. This experiment gives a positive indication of the possibility of nitriding and the hardness change for Titanium.

4.4 Modification of Steel Surface

In this section, a similar experiment to previous section has been carried out with steel. A similar objective was set for coating steel substrate with its nitride under direct firing of the plasma focus. The objective of this experiment is to see whether the treatment from the plasma focus can be used to change the surface of steel to have a desired property [28].

In this first test, a steel plate was placed at 13 cm from the end of the anode. The plasma focus was fired under an operating pressure of 0.5 mbar for sixty shots. The color change of the steel surface can be observed. Again it is suspected that this change may be caused by the high energy ions from the focusing process other the heating of the steel by the plasma jet. The color change is shown in Figure 4.15.

Figure 4.15: A picture of a steel plate taken before and after the firing of the plasma focus [28].

The hardness test was also performed on the sample. The result from a Rockwell (Scale B) hardness test on the sample surface is shown in Table 4.3. The surface of the sample was also observed with SEM and the composition was tested with EDX. The result are shown in Figure 4.16 and Figure 4.17.

Sample	Hardness Rockwell Scale B (HRB)
Before	71.86+1.070
After	68.62+0.741

Table 4.3: A table showing the result of the hardness test (by Rock well scale B (HRB)) on the steel plate after plasma focus treatment [28].

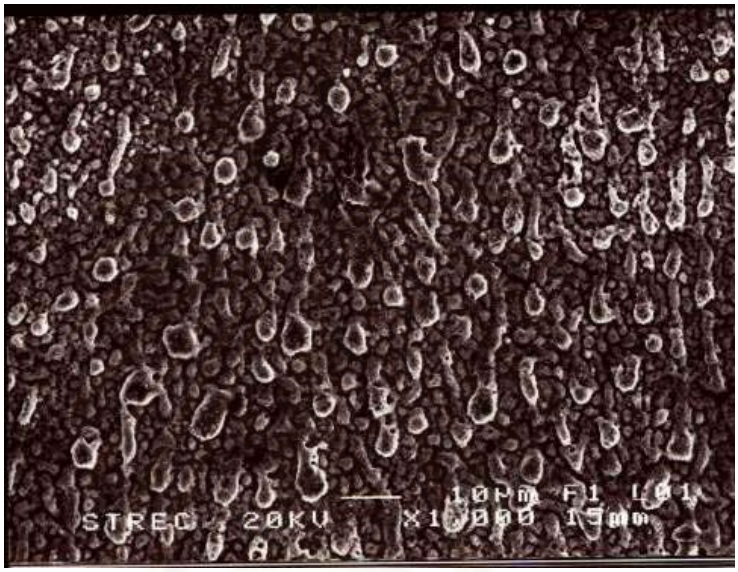

Figure 4.16: An enlarged (x1,000) picture of the surface of the steel plate after the bombardment of the plasma focus taken by SEM [28].

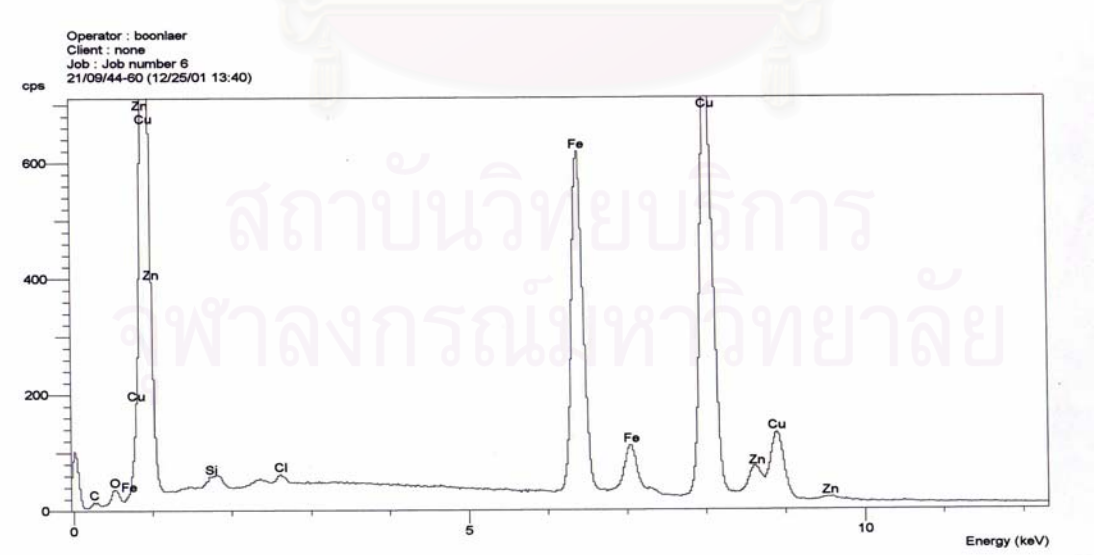

Figure 4.17: A graph showing the result from EDX of the steel plate showing a clear trace of copper [28].

On the surface, it can be seen from SEM that there is a coating layer. This coating layer is in a form of close packed droplets. EDX shows that there are traces of copper. The copper is expected as previously discussed. There are no traces of nitride. From the hardness test result, it seems that the sample became softer. A possible explanation for this is the coating of the surface. If the surface is coated with copper then it is possible that, when the hardness probe is pressed on the sample, this coated surface absorb the force of the probe causing the measurement to read softer. In the second experiment, another steel sample was tested. It was placed at 11 cm from the end of anode, and operated under 1 mbar pressure. Fifty shots were fired.

Figure 4.18: A picture of a steel plate taken before and after the firing of the plasma focus [28].

A similar result is shown in Figure 4.18. There are some copper coated area and some area with color changes. As discussed before this copper coated is expected due to the corrosion of the anode. The color change of the surface is more likely caused by the heating of the plasma. They yielded similar result as the previous experiment. SEM image is shown in Figure 4.19. For the EDX there were no trace of nitride observed. This is shown in Figure 4.20. In order to obtain proper nitride for steel, one must study deeper into the chemical process of steel nitride formation. Specific nitriding steel must be used for a successful nitriding.

Figure 4.19 : An enlarged (x15,000) picture of the surface of the steel plate after the bombardment of the plasma focus taken by SEM [28].

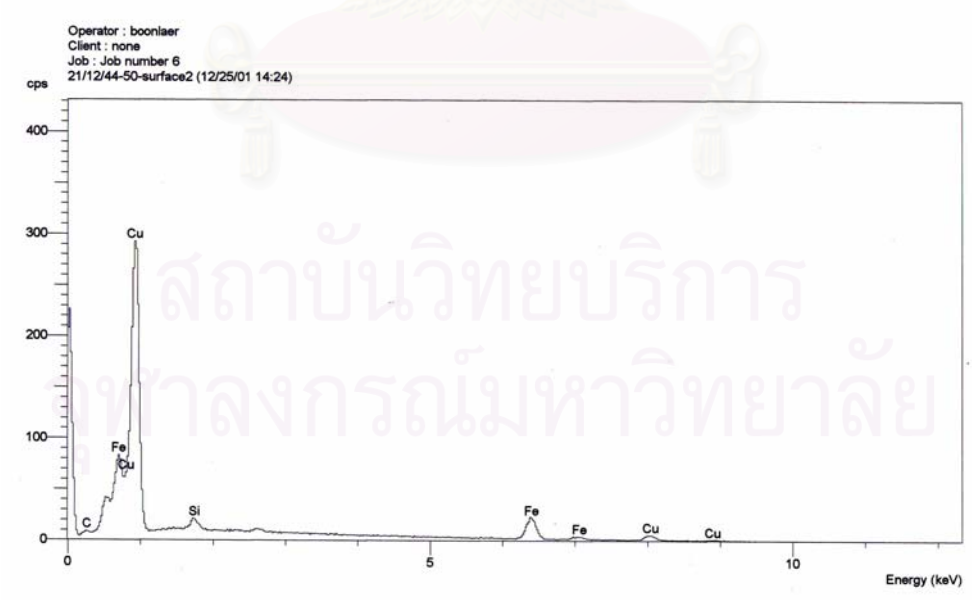

Figure 4.20: A graph showing the result from EDX of the steel plate showing a clear trace of copper [28].

In summary, an overview of plasma focus effects on material surfaces were observed. When the plasma is operating in a focusing mode, it is more likely to cause some degree of damage to the surface which depends upon the type of material. On the other hand this mode of operation is the most effective to surface coating where the coating material can be placed at the tip of the anode. An appropriate plasma focus configuration must be used for optimum coating on the material otherwise the damaging effect can cause an undesirable result to the coating process.

For the non-focusing mode, the damage on the material surface is far less. Only the heating effect on the material surface is observed.

CHAPTER 5

CONCLUSION AND DISCUSSION

5.1General Conclusion

The mechanism and operating conditions of the plasma focus device have been studied experimentally. Several diagnostic techniques have been used to measure the characteristic of the plasma and the plasma focus, such as voltage and current signal measurements, plasma sheath velocity measurement, plasma jet velocity.

It was found that the optimum operating pressure for the plasma focus device is in the range of 0.5 mbar to 9 mbar. The charging voltage is 12.5 kV. From the voltage signal measurement (Figure 3.2) the breakdown peak voltage is 7.28 kV. There is a reduction of voltage by 42%. This may be caused by the inefficiency in the discharging process through the spark gap switch.

The average speed of the plasma sheath can be estimated from the voltage signal at a pressure of 0.5 mbar to be 4.514 cm/μs and deceases when the pressure increases as shown in Section 3.1. The voltage signal for the short anode shows good focusing signal for Nitrogen gas when the pressure range is between 0.5 mbar to 2.5 mbar and with the range between 0.5 mbar to 2.0 mbar for Argon gas. The long anode produces good focusing peak when Nitrogen gas pressure is between 0.5 mbar to 1.5 mbar and 0.5 mbar to 1.5 mbar for Argon gas.

For the current measurement, the maximum current measured during the discharge is 136.77 kA where the current/voltage conversion factor K is 7.275 for the set up. From a series of experiments, it is obvious that the voltage and current flow in plasma also depend on the gas fill in the plasma focus tube.

It was also found that average speed of the plasma sheath in Nitrogen is faster than that in the Argon gas. This can be explained by the different in the molecular weight of the gases. Argon has a molecular weight of 40 while Nitrogen has a molecular weight of 14 [16].

From the plasma focus dynamics simulation, the characteristics of the plasma focus can be deduced. The measured velocity and the calculated velocity are found to be in good agreement. This confirms a certain degree of accuracy to the Slug model used for axial phase calculation. The characteristics of the plasma focus is shown in Table 5.1 below.

Type characteristic	result
Inducticity (Lo)	127.33 nH
Capacity	30 μF
Discharge characteristic time (t_o)	1.9545 μs
K-factor	7.275 kA/V
Maximum current	136.77 kA
Range center of anode to cathode(b)	3.2 cm.
Radius of anode(a)	0.95 cm.
Length of anode (Zo)	16.0 cm.
Resistance of plasma focus (ro)	0.012 Ω
Mass factor (MASSF)	0.045
Current factor (CURRF)	0.7
Mass flow current (MASSFR)	0.16
Voltage input (Vo)	13 kV
Moleclular weight of Nitrogen gas	14

Table 5.1:The characteristic of plasma focus use in experiment.

The average velocities of current sheath at pressure ranging from 0.5 mbar to 3 mbar of Nitrogen gas is between 6.855 cm/μs to 1.789 cm/μs. The average velocity for Argon gas in same pressure range is between 6.380 cm/μs to 1.645 cm/μs. The velocities of the plasma sheath from the simulation is within the error bar of the measured velocity.

In the studies of the plasma jet, it was found that the plasma focus device can produce plasma jet in two cases. The first case is when the plasma focus is operated in a focusing mode and the second case is when it is operated in a non-focusing mode. When there is a focus, then there is more ions emission which are suspected to have more energy than that of the plasma jet. This can be seen from the signal in Section 3.5. The average velocities of the plasma jet are found to be between 0.4268 cm/μs and 0.0365 cm/μs. The velocity of the plasma jet behaves in a similar way as the velocity of the plasma sheath. As the ambient pressure increases the velocity decreases.

5.2 Conclusion for Material Surface Modification

Different types of materials were investigated under the plasma focus modification process, which are insulating and conducting substrates. The modification process is based on the used of the plasma jets, high energy ions, high energy electrons and the metallic vapor released by the axial rundown phase or the electron bombardment to the anode. The modification process was found to modify the material surface in two ways. Firstly, the process can produce a coating of the metallic vapor on both insulating and conducting substrate. Secondly, the process can also cause an undesirable damage to the surface of both type of substrate. The

conditions which dictate the coating or the damaging process are the position of the substrate with respect to the anode and the focusing of the plasma. As seen from the experiment in Chapter 4, the damage can be caused when the plasma is strongly focused and that the substrate is placed near the anode where the focus occurs. The focusing process can be controlled by adjusting to an appropriate pressure as described in Chapter 3.

On the other hand, the coating process works well when there is a focus also, since the metallic vapor depends, predominantly, on the high energy electron bombardment. Therefore, in order to obtain a good coating, a correct substrate position is essential. It was found that the position of substrate must be a good distance away from the focusing point and possibly at an angle away from the axis of the anode. A reasonable coating of copper was observed with glass substrate. Some copper was also observed on conducting samples.

If the substrate is at a longer distance away, it is likely that the surface is affected by the plasma jets are the high energy ions. It was found that the plasma jets or the ions can, at this time, contribute very little to the surface modification. With is set up, the energy of the plasma jet a ion required to cause the change on the surface of some materials tested may not be enough, therefore only heating effect was observed in the experiment with Ti and steel plates. No trace of nitriding can be detected. With the hardness test, there are some changes which can be observed on both, Ti plate and the steel plate. For the Ti plate, the hardness reading increases, but this is still inconclusive that the hardness is caused by the nitride. On the other hand, for the steel plate, the hardness is less. This is clearly due to the layer of copper which

is coated on the surface. The evidence of copper coating was clearly observed by the EDX.

One can conclude that the plasma focus can be used to modify material surface. The quality of the coating and the extent of the damage can be controlled by the set up and then operating condition of the plasma focus. It is interesting to make further study of these conditions in order to obtain a reliable method of surface modification.

5.3 Suggestion and Future Work

With the time given, this research work yield an extensive study of the UNU/ICTP plasma focus system and its operation and also a preliminary study of how to modify the plasma focus for material surface modification purpose. It is interesting to further study other possible configuration for surface modification by using the plasma jet and the ions produce from the plasma focus. In order to make use of the ions, the plasma focus must be operated under a lower pressure. This will increase the mean free path of both the plasma jet and the ions.

Better diagnostics technique should be developed in order to detect the ions or the plasma jet. An ultra fast picture of the surface modification by the plasma should be taken in order to provide more information about the process.

REFERENCES

1. AAAPT. TWELVE YEARS OF UNU/ICTP PFF-A REVIEW, The United Nation University: 1963.
2. Hétor Kelly, Alejandro Lepone, Adriana Márquez, Marek J. Sadowski, Jaroslaw Baranowski, and Elzbieta Skladnink-Sadowska. Analysis of the Nitrogen Ion Beam Generated in a Low-Energy Plasma Focus Device by a Faraday Cup Operating in the Secondary Electron Emission Mode. IEEE Transaction on Plasma science Vol. 26, No.1,February 1998.
3. Hong-Xia Zhang, Ying-Bing Jiang, Si-Ze Yang, Zhangda Lin, and Ke-am Feng. Diamond growth on steel substrates with AL-N interlayer produced by high power plasma stream. Thin Solid films 349(1999): 162-164.
4. Chhaya R. Kant, M.P. Srivastava, and R.S. Rawat. Thin carbon film deposition energies ions of dense plasma focus. Physics letter A 226(1977): 212-216.
5. B.B. Nayak, B.S. Acharya, S.R. Mohanty, T.K. Borthakur and H.Bhuyan. Surface nitriding of graphite substrate by plasma focus device towards synthesis of carbon nitride coating. Surface and Coating Technology 145 (2001):8 –15.
6. H. Kelly, A. Lepone, A. Márquez, D. Lamas and C. Oviedo. Coating on metallic samples produced by a small energy plasma focus. Plasma Source Sci. Technol 5 (1996): 704-709.
7. Ruby Gupta, Rachna Garg and M.P. Srivastava Titanium Carbide Film Deposition Using Dense Plasma Focus Proc. Regional Conf. on Plasma Research in 21st Century (2000): 128-131.
8. Z. Werner, J. Piekoszewski, and W. Szymczyk. Genration of high-intensity pulsed ion and plasma beams for material processing. Vacuum Surface Engineering, Surface Instrumentation & Vacuum Technology 63 (2001): 701-708.
9. A. Lepone, H.Kelly, D. Lamas, and A. Marquez. Surface modification produced by nitrogen operated plasma focus device: the role of the ion beam in the heating of a substrate. , Applied Surface Science 143 (1991): 124-134.
10. Bin Liu, Chizi Liu, Xiangjun He, Dajun Cheng, Rui He, and Si-Ze Yang. Pulsed High energy Density plasma (PHEDP) Processing Ceramic Surface. Proc. Regional Conf. on Plasma Research in 21st Century (2000): 132-136
11. R.S. Rawat , W.M. Chew, P. Lee,T. White ,Bing Shan, S.P. Moo and S.Lee. Room Temperature Growth of Titanium Nitride Thin Film on Stainless Steel Substrates Using Plasma Focus Device. Proc. Regional Conf. on Plasma Research in 21st Century (2000): 122-127.
12. P.Kamsing. A Study of Coating Method for Polymer by using Plasma Focus Device. Bachelor Report, Department of Physics, Faculty of Science, Chulalongkorn University, 2000.
13. S. Lee, B.C. Tan, C.S. Wong, and A.C. Chew. Laser and plasma Technology. Proc. Second Tropical College on Applied Physics: World Scientific, 1986.
14. C.S. Wong. SMES4308: Plasma Devices, Plasma Focus. Physics Department University of Malaya: C.S. Wong, 1986.

15. C. Chaimongkol. Development of Charger for High Voltage Capacitor Bank for Plasma Focus Device. Bachelor Report, Department of Physics, Faculty of Science, Chulalongkorn University, 1999.
16. A.H. Beck Handbook of vacuum Physics Volume 2. Library of Congress Catalog Card No. 63-21443.
17. P. Maneerat. Development Plasma Focus Device. Bachelor Report, Department of Physics, Faculty of Science, Chulalongkorn University, 1999.
18. Kazuto Takao, Yasuhiko Doi, Satoshi Hirata, Masaki Shiotani, Iwao Kitamura, Takazu Takahashi, and Katsumi Masugata. Characteristic of Ion Beams Produced in a Plasma Focus Device. Jpn. J. Appl. Phys. Vol. 40 (2001):1013-1015.
19. Yakov E. Krasik and Amit Weingarten. Energetic Electron and Ion Beam Generation in Plasma Opening Switch IEEE Transactions on plasma science, Vol 26, No. 2, April 1998.
20. L. Jakubowski, M. Sadowski and J. Zebrowski. Measurements of Charged Particle Beam from Plasma-Focus Discharges. To be published.
21. M. Scholz, L. Karpinski, W. Stepniewski, A.V. Branitski, M.V. Fedulov, S.F. Medovschikov et al. Foam liner driven by a plasma focus current sheath. Physics Letters A 262(1999): 453-456.
22. Low Yoon Keong. Ion Beam emission from plasma focus device. Master Degree Department of Physics, Faculty of Science University of Malaya, Malaysia, 2002.
23. V.I.Krauz, V.V.Myalton, E.Yu.Khautiev, V.P.Smirnov,A.N.Mokeev, M.A. Karakin et al. PLASMA FOCUS RESEARCH AT THE KURCHATOV INSTITUTE. Institute for High Energy Densities of Associated Institute for High Temperatures Russian Academy of Sciences, Moscow: 1999.
24. R. H. Huddlestone and S. L. Lenard. Plasma Diagnostic Techniques. Academic Press: 1965.
25. M. Zakaullah, Imtiaz Ahmad, G. Murtaza, and M.M Beg. Influence of Magnetic Probe Presence on Current Sheath Dynamics in Plasma Focus Operation. Fusion Engineering and Design 36 (1997): 437-442.
26. C.T. Chang, M. Hashmi and H.C. Pant. Study of a Laser-Produced Plasma by Langmuir Probes. Pergamon press Vol. 19 (1977) :1129-138.
27. S. Tung. Determination of Plasma Temperature and Speed of The Plasma Sheath Produced by Plasma Focus Device from Plasma Induced X-Ray Photon. Bachelor Report, Department of Physics, Faculty of Science, Chulalongkorn University, 2000.
28. T. Lalitkulthorn. Preliminary Study of Steel Surface Modification by Nitrogen Plasma from Plasma Focus Device. Bachelor Report, Department of Physics, Faculty of Science, Chulalongkorn University, 2001
29. www.calce.umd.edu/general/Facilities/Hardness.html.

APPENDIX A

CIRCUIT ATTENUATOR

A1 Attenuator X10

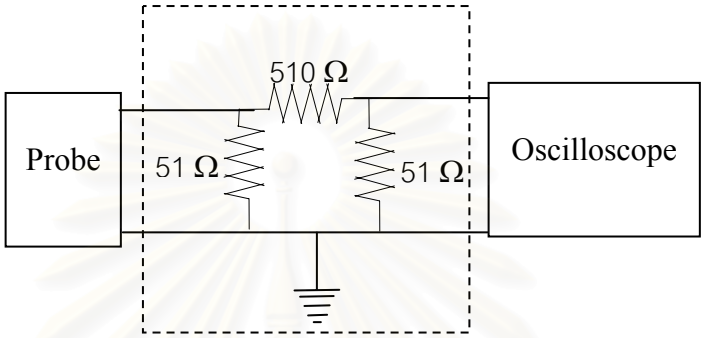

Figure A1: Attenuator x 10

A2 Attenuator X1

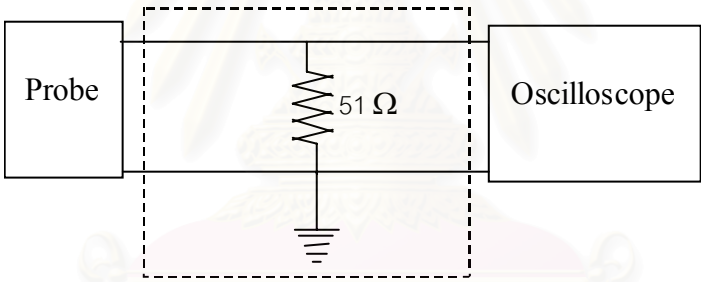

Figure A2: Attenuator x 1

A3 Bias Circuit

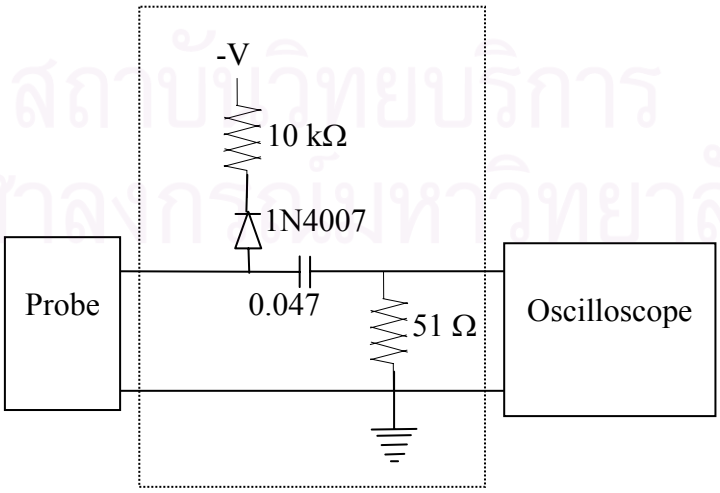

Figure A3: Bias circuit used in the Lab at University of Malaya, Malaysia.

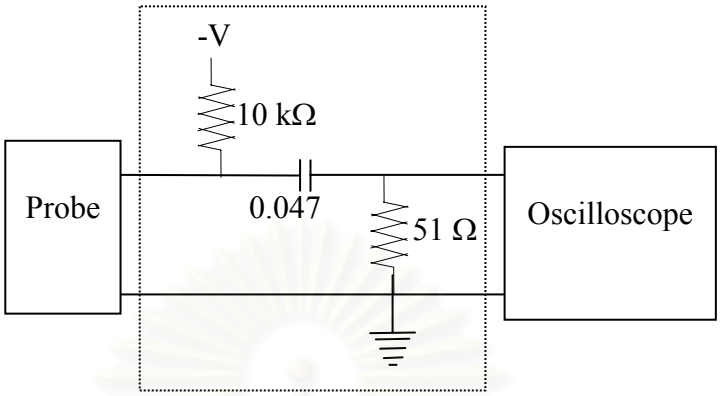

Figure A4: Bias circuit used in the Lab at Chulalongkorn University.

A4 Integrator

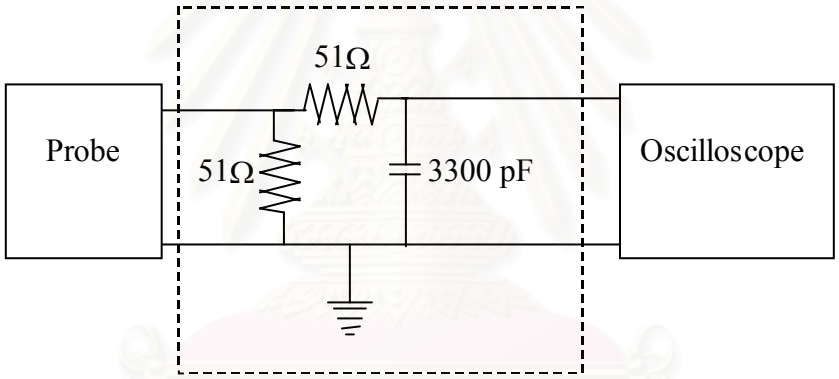

Figure A5: Circuit of an integrator.

APPENDIX B

PIN-DIODE BPX-65

B1 Parameters of Pin diode (BPX-65)

Effective detection area	1 mm^2
Intrinsic Si wafer thickness (estimated)	~ 10 μm
Dead layer thickness (estimated)	~ 5 μm
Rise time (typical)	0.5 ns

Each diode is contained inside a TO-18 casing with a glass window.

APPENDIX C

HARDNESS TEST

C1 Vickers Hardness Test [29]

It is the standard method for measuring the hardness of metals, particularly those with extremely hard surfaces: the surface is subjected to a standard pressure for a standard length of time by means of a pyramid-shaped diamond. The diagonal of the resulting indention is measured under a microscope and the Vickers Hardness value read from a conversion table

Vickers hardness is a measure of the hardness of a material, calculated from the size of an impression produced under load by a pyramid-shaped diamond indenter. Devised in the 1920s by engineers at Vickers, Ltd., in the United Kingdom, the diamond pyramid hardness test, as it also became known, permitted the establishment of a continuous scale of comparable numbers that accurately reflected the wide range of hardness found in steels.

The indenter employed in the Vickers test is a square-based pyramid whose opposite sides meet at the apex at an angle of 136^0. The diamond is pressed into the surface of the material at loads ranging up to approximately 120 kilograms-force, and the size of the impression (usually no more than 0.5 mm) is measured with the aid of a calibrated microscope. The Vickers number (HV) is calculated using the following formula:

$$HV = 1.854(F/D2),$$

with F being the applied load (measured in kilograms-force) and D2 the area of the indentation (measured in square millimeters). The applied load is usually specified when HV is cited.

The Vickers test is reliable for measuring the hardness of metals, and also used on ceramic materials. The Vickers testing method is similar to the Brinell test. Rather than using the Brinell's steel ball type indenter, and have to calculate the hemispherical area of impression, the Vickers machine uses a penetrator that is square in shape, but tipped on one corner so it has the appearance of a playing card "diamond". The Vickers indenter is a 136 degrees square-based diamond cone, the diamond material of the indenter has an advantage over other indenters because it does not deform over time. The impression left by the Vickers penetrator is a dark square on a light background. The Vickers impression is more easily "read" for area size than the circular impression of the Brinell method. Like the Brinell test, the Vickers number is determined by dividing the load by the surface area of the indentation (H = P/A). The load varies from 1 to 120 kilograms. To perform the Vickers test, the specimen is placed on an anvil that has a screw threaded base. The anvil is turned raising it by the screw threads until it is close to the point of the indenter. With start lever activated, the load is slowly applied to the indenter. The load is released and the anvil with the specimen is lowered. The operation of applying and removing the load is controlled automatically.

Several loadings give practically identical hardness numbers on uniform material, which is much better than the arbitrary changing of scale with the other hardness machines. A filar microscope is swung over the specimen to measure

the square indentation to a tolerance of plus or minus 1/1000 of a millimeter. Measurements taken across the diagonals to determine the area, are averaged. The correct Vickers designation is the number followed "HV" (Hardness Vickers). The advantages of the Vickers hardness test are that extremely accurate readings can be taken, and just one type of indenter is used for all types of metals and surface treatments. Although thoroughly adaptable and very precise for testing the softest and hardest of materials, under varying loads, the Vickers machine is a floor standing unit that is rather more expensive than the Brinell or Rockwell machines.

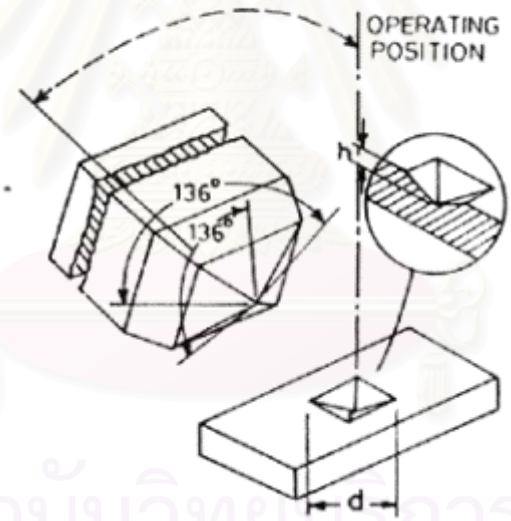

Figure C1 Model of Vicker Hardness.

APPENDIX D

PLASMA FOCUS COMPONENTS

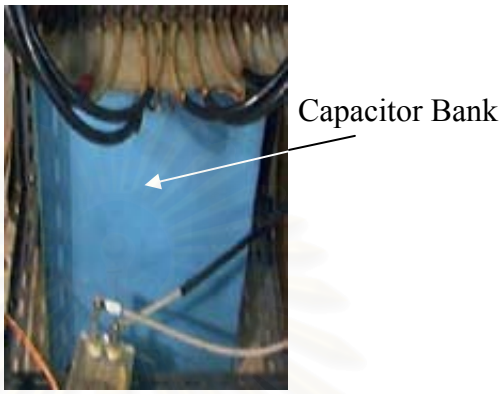

Figure D1: The capacitor bank.

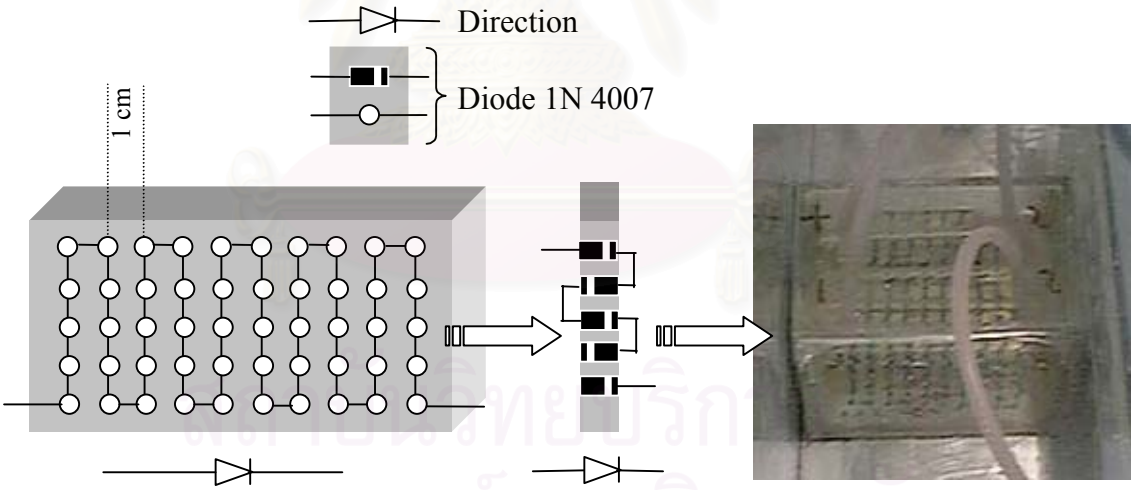

Figure D2: Bridge Rectifier.

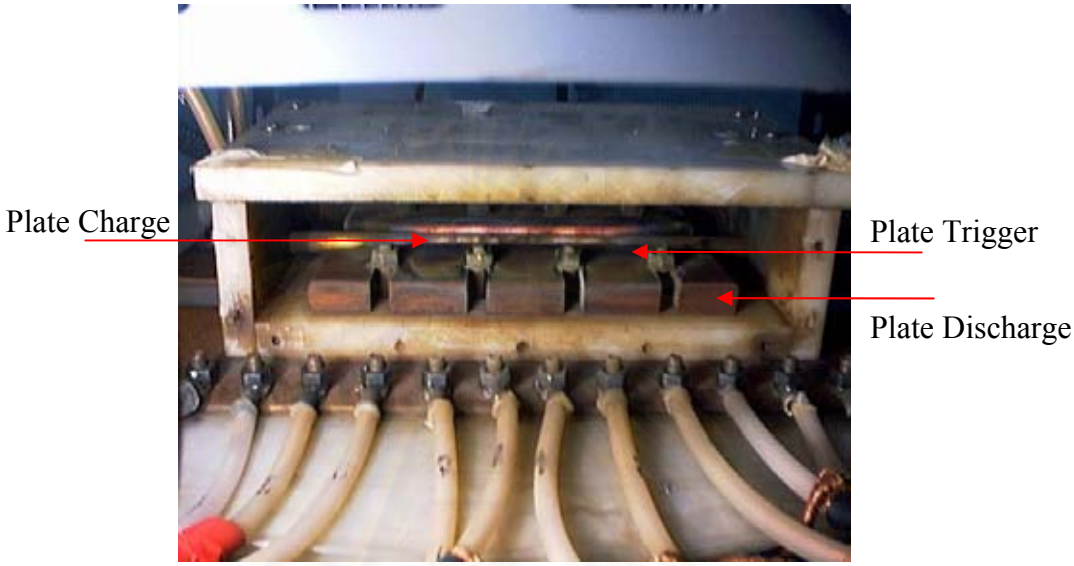

Figure D3: Subsystem: Spark Gap Switch.

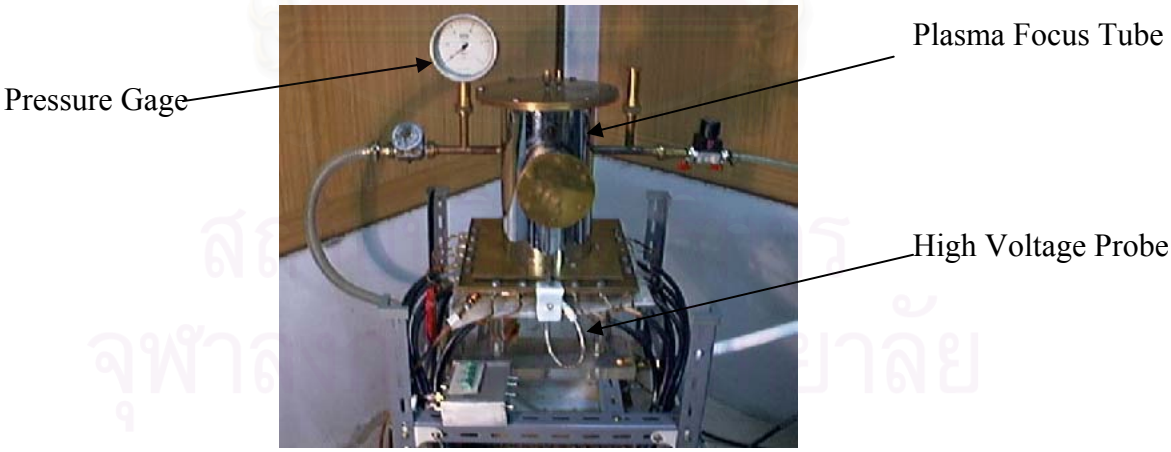

Figure D4: A picture showing pressure gauge, plasma focus tube and high voltage probe.

BIOGRAPHY

NAME MR.DUSIT NGAMRUNGROJ

BIRTH 16 NOVEMBER 1977

EDUCATION 2000 – Present M.Sc. Physics , Department of Physics, Faculty of Science, Chulalongkorn University, In 1996 - 1999 Bachelor's Degree from Chulalongkorn University, gpax 3.06, In 1990 - 1995 High School at Angthong Patthamarot Wittayakhom, gpax 3.26,In 1984 – 1989 Primary School at Anubanwat Angthong

PUBLICATION - Final year project report, "Development of an Electronics Circuit for Controlling High Voltage Charger", 1999

SCHOLARSHIP - Young Scientist Development program 1999
- Oct-2001 Unesco and AAAPT for experiment at University of Malaya, Malaysia

WORK EXPERIENCE

-Teaching Assistant – Undergrduate level at Chulalongkorn University and Asian University of Science and Technology, 2001-Present

-Teaching Assistant – High School Level, 2000

-Organising Comittee for Plasma Physics Conference 2000 and 2001

-Organiser for Chulalongkorn University Science Fair 1996 and 1999

-Tutor in Chulalongkorn University Undergraduate Tutorial Program 1998-1999

-Organiser for Undergraduate Orientation Camp 1996-1998

-Representative of Angthong Patthamarot Wittayakhom High School for Science Competition 1995

-Training the plasma focus for plasma jet, 1 October 2001 to 28 December 2001 at University of Malaya, Malaysia

-Training the plasma focus for gem stone, 28 may 2002 to 8 June 2002 at University of Malaya, Malaysia

-Teaching Assistance first year lab for Undergraduate at Chulalongkorn University in 2001 and 2002

-Seminar 20-22 March 2002, Science Fair in Chulalongkorn University

-1996 to 1999 Staff the football tradition of Chulalongkorn University and Thammachat University